Minor project Sustainable Energy Systems
Project Report on

ENERGY INDEPENDENT SYSTEM FOR RESIDENTS AT THE ROSANDEPOLDER

Authors:

Sanjaya Ghimire	*2119886*
Jahangir Hossein Shah	*2124524*
Farhan Nazir	*2122432*
Yang Hong	*2120355*

Supervisors:
Karl Wallkum
Miel Stapel

Client:
Residents of Rosandpolder

June 8, 2024

Preface

Sustainable energy systems is one of the Master's in Engineering system's elective modules at HAN University of Applied Sciences. As part of a minor project in this module, a group of students have chosen the project Energy Independent System for Residents at the Rosandepolder in order convert the community of Rosandpolder into self sustainable energy independent.
The students were successful to deliver the model of the system designed for achieving energy independence with the help of Karl Wallkum and Meil Stapel as their project supervisor and Hans Meerman as an advisor from HAN University of Applied Sciences. The project group would also like to acknowledge the residents of Rosandepolder for their enthusiasm and efforts in supporting the project's success.

Summary

The objective of this project is to design an energy-independent system for the Rosandepolder community by integrating renewable energy sources with battery and hydrogen-based storage solutions. The goal is to create a self-sustainable energy system that meets the community's energy demands while aligning with sustainability goals and reducing reliance on fossil fuels.
The methodology involved a comprehensive analysis and simulation of different energy scenarios using solar photovoltaic (PV) panels and wind turbines as primary energy sources. Three scenarios are analyzed: Scenario 1, which utilized only PV panels; Scenario 2, which combined PV panels with a wind turbine; and Scenario 3, which accounted for additional heating needs using heat pumps. The study focused on determining the optimal specifications for the energy storage components, including battery capacity, hydrogen electrolyser capacity, hydrogen storage capacity, and fuel cell capacity. The system's economic feasibility was assessed through net present value (NPV) and payback period calculations.
The conclusions drawn from the study indicated that integrating solar PV panels and wind turbines was the most effective combination of renewable energy sources. The optimal battery capacity ranged from 300-700 kWh, depending on the scenario, with lithium-ion technology being preferred. The hydrogen storage system, with an electrolyser capacity of 100-140 kW and a storage capacity of 8,000-26,000 litres, ensured long-term energy storage, while the fuel cell capacity ranged from 45-70 kW. Scenario 2 presented the best economic outcome with a positive NPV and the shortest discounted payback period, indicating economic sustainability.
Overall, the project demonstrated that an energy-independent system for the Rosandepolder community is technically and economically feasible through the strategic integration of solar PV, wind energy, and hybrid storage solutions, successfully meeting energy demands and contributing to sustainability goals.

List of Figures

Contents

1 Introduction

1.1 Background

The Rosandepolder community is committed to attaining energy independence, understanding the crucial part that plays in promoting sustainability and resilience to the rising environmental problems and energy limitations. This move towards independence contributes the energy transition and also align with the Dutch government's policy to cut greenhouse gas (GHG) emissions by 49% by 2030 and by 95% by 2050 (van Economische Zaken en Klimaat, 2019). The concept of energy independence lead us to the need for renewable energy sources to primarily cater for our energy needs (Dwivedi, Sudhakar, Soni, Solomin, & Kirpichnikova, 2020). These non-conventional sources include solar, wind, tidal and biomass energy. Solar technology stands out among these because it is readily available and produces clean energy (Parthiban & Ponnambalam, 2022)
Each of these sustainable energy sources offers unique advantages and challenges, and the selection of energy sources for an energy-independent system should consider factors such as resource availability, reliability, environmental impact, and technological feasibility(Jacobson, 2009).
Achieving complete energy independence through sustainable energy sources requires overcoming the significant challenge of energy storage. This entails ensuring that sufficient energy is stored within the system to provide power even during periods and throughout seasons when the sun isn't shining or the wind isn't blowing thereby ensuring flexibility and reliability in powering households. Thus,integrating multiple renewable energy sources and implementing energy storage solutions can help mitigate the limitations of individual energy sources and ensure a reliable and sustainable energy supply(Díaz-González, Sumper, Bellmunt, & Villafafila-Robles, 2012).
Rosandpolder community is a group of 43 beautiful floating houses build over the water located south of southeast of Oosterbeek just east of the Arnhem-Nijmegen railway line in the Netherlands (*Rosandepolder*, 2023). The residents of the Rosandpolder community are willing to establish the energy independent system. As a result, a team of sustainable energy systems engineering students at HAN University of Applied Sciences has accepted the challenge to design and deliver the optimal self-sustainable solution to meet the energy demand of the Rosandpolder community.

The project location is as shown in the figure 1 below:

Figure 1: Google Map view of Rosandpolder community (Project Location)

1.2 Problem definition

The type of renewable energy sources and its quantity dictates the configuration and specification of hydrogen combined with battery based energy storage system. To create a energy independent system for the community of Rosandpolder, the energy production , storage and usage should be balanced. This will be the main focus of this project , where it is unclear what types and quantity of renewable energy sources integrated with what size and specifications of battery and hydrogen based energy storage will be sufficient enough to fulfil the energy demand of the community of Rosandpolder. Additionally, project also determines whether the overall system is economically viable or not. The diagram in figure 2 represents the major components of the total system. The aim of the project is to design a solution that eliminates the community's reliance on the national grid.

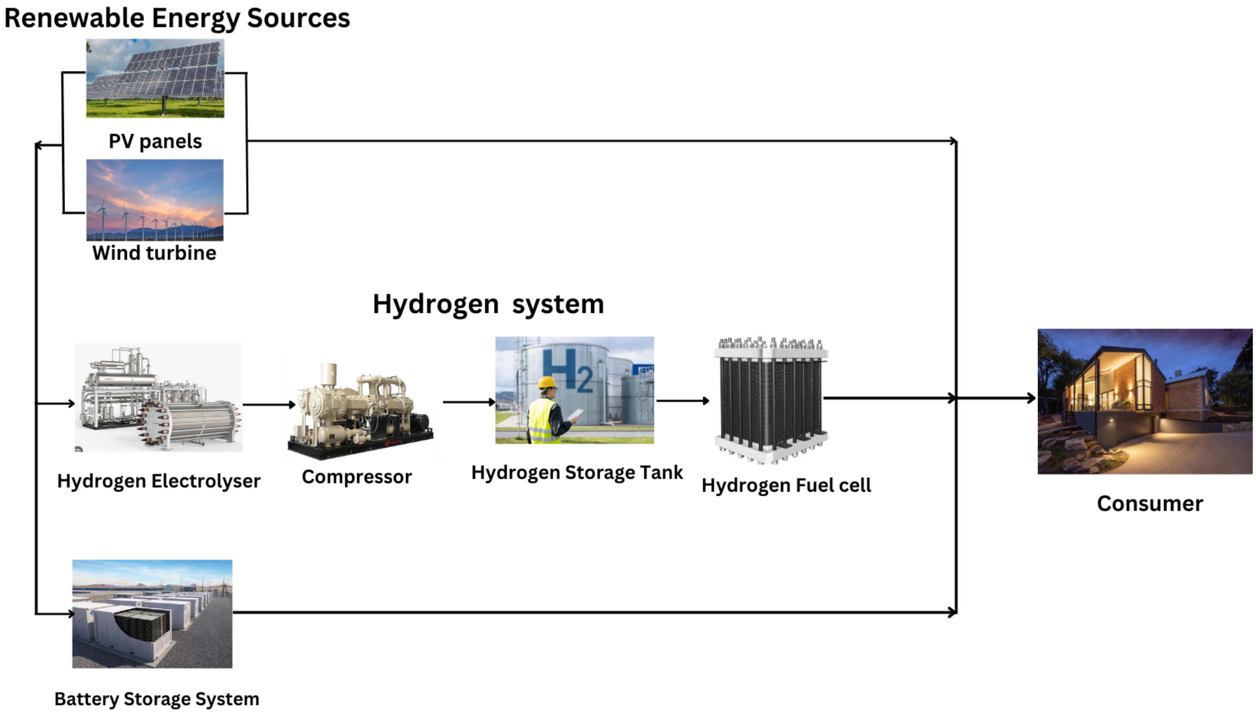

Figure 2: Schematic diagram of major components of the proposed system(*Edited in canva.com*, n.d.)

1.3 Project objectives

The project's primary objective is to design a self-sustainable energy system for the Rosandepolder community, focusing on balancing energy production and storage for fulfilling the energy demand. For this, following sub-objectives should be achieved:

1.3.1 Sub-objectives

1. Collect and analyse the current energy production and demand of the community.
2. Analyse and predict the future energy demand of the community.
3. Determine the appropriate types and quantities of renewable energy sources.
4. The specification and sizing of battery and hydrogen-based energy storage systems.
5. Evaluate the economic feasibility of the developed solution.

1.4 Research question

The research question of the project is as follows.
What is the ideal combination of energy sources integrated with battery and hydrogen based storage, to have an energy independent system for the Rosandepolder?

The following research sub-questions will help answer the main research question.

1.4.1 Research Sub-Questions

1. *What is the current energy demand and production of the client?*
2. *What is the type and optimal number of energy sources to meet the energy requirements of the client?*
3. *What is the optimal specification and size of the battery storage?*
4. *What is the optimal specification and size of hydrogen electrolyser?*
5. *What is the optimal specification and size of the hydrogen storage tank?*
6. *What is the optimal specification and size of hydrogen fuel cell?*
7. *Is the solution economically viable?*

1.5 Outline of the Minor Project Report

Chapter 2 discusses the literature review. Chapter 3 describes the complete methodology regarding the mathematical modelling and all the involved differential equations. Chapter 4 describes scenarios of simulation and its corresponding results and validation of results. The conclusion is given in chapter 5. Finally the recommendations resulting from the project are summed up in chapter 6. At the end the references and appendices can be found.

2 Literature Survey

To begin with, literature survey is performed to gain understanding of the concepts, how hydrogen based off-grid system work and requirement of transition to independent system.

2.1 Off-grid electricity system and its importance in energy transition

Renewable electricity production in the Netherlands is on a swift upward trajectory each year. In 2023, it surged by 21 percent compared to the previous year. This growth coincided with a decline in the proportion of electricity generated from fossil fuels. Additionally, the Netherlands achieved record-high electricity exports to neighbouring countries. Notably, in 2023, 48 percent of electricity was generated from renewable sources such as solar, wind, and water (Netherlands, 2024) as shown in figure (3) below. For the Netherlands, this trend of increase in renewable energy production is in line with (van Economische Zaken en Klimaat, 2019), which in alignment with international Paris Agreement (for Climate & Solutions, 2019).

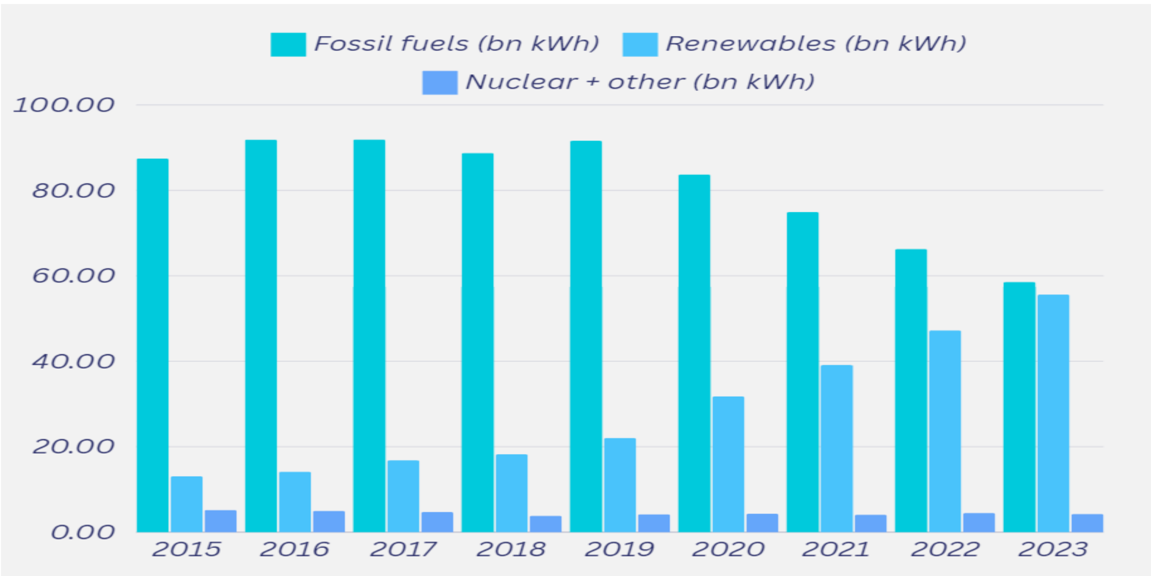

Figure 3: Electricity production by source (Netherlands, 2024)

However, this increase in renewable electricity production impose challenges regarding electricity supply demand mismatch and grid instability (Nortier et al., 2023). The difference between energy demand and supply may lead to instances of electricity grid overload during summer or daytime periods, as well as potential energy supply deficits during winter, cloudy days, or nighttime, creating a mismatch between energy demand and supply (Mertens, 2022). And, the grid instability is because these forms of renewable energy lack the rotational inertia characteristic of traditional synchronously-connected generators, potentially leading to decreased overall stability of the grid (Johnson, Rhodes, & Webber, 2020).

A solution to both of the problem is the development of micro-grids: localized energy grids capable of managing supply and demand through the utilisation of available energy resources (Metabolic, 2020). For only electricity under consideration, specially with PV only as renewable source three types of system can be implemented : 1) grid-tied system, 2) off-grid system, 3) hybrid system (Hyder, n.d.). As name suggests off-grid system has no connection to the national grid at all also called as standalone system.

2.2 Renewable energy sources

The amount renewable energy in account for total energy consumption in the Netherlands is increasing per year. In 2022, share of renewable energy in total national energy consumption was 15% as shown in figure 4. And among energy sources solar energy consumption increased by 45% and wind energy consumption by 13% in 2022 as shown in figure (5) (Netherlands-Statistics(CBS), 2023)

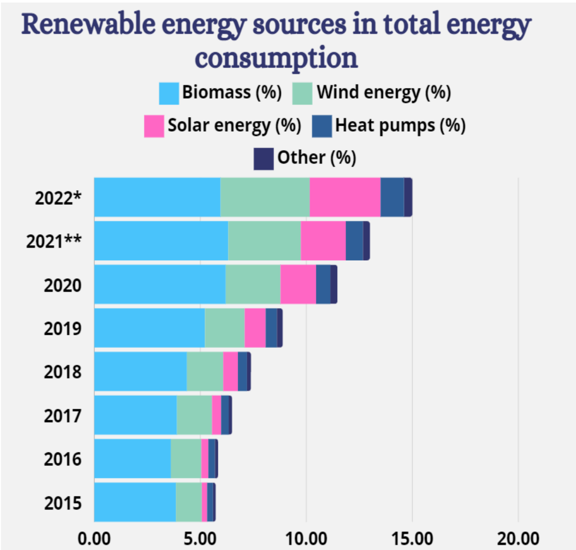

Figure 4: Share of renewable energy in total energy consumption (Netherlands-Statistics(CBS), 2023)

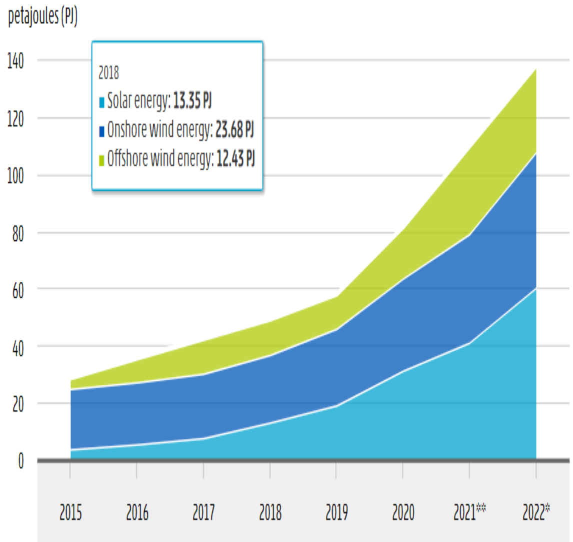

Figure 5: Wind and solar energy consumption (Netherlands-Statistics(CBS), 2023)

2.2.1 Photovoltaic panel

The fundamental principle behind solar photovoltaic (PV) energy lies in the direct conversion of sunlight into electricity by the PV effect using solar cells (El Hammoumi, Chtita, Motahhir, & El Ghzizal, 2022).The research of modelling the dynamic behaviour of PV Power generation includes different factors like accurately capturing the effects of solar irradiance, temperature and other environmental factors (Parthiban & Ponnambalam, 2022). The amount of sunlight that hits a solar panel is one of the biggest factors in how much electricity it can produce. Other main factors are panel and system characteristics, roof orientation and panel's age (Lane, n.d.).

2.2.2 Wind Turbine

The fundamental principle of wind turbines lies in the conversion of the mechanical power of the wind to electrical power considering the aerodynamic power efficiency, mechanical efficiency and generator efficiency (Thapar, Agnihotri, & Sethi, 2011). In practice, wind turbines are unable to harness more than 59.3% of the energy present in the wind, a limitation referred to as the Betz limit (Carriveau, 2011). The characteristics of the blades play a crucial role in determining the energy extractable from the wind. Therefore, enhancing the performance of a wind turbine blade directly boosts the efficiency of the wind turbine (YİĞİT, 2017).
Wind turbines can be classified as low-speed or high-speed based on their design and operating characteristics. Low-speed turbines have longer blades, lower cut-out speeds around 12-13 m/s, and generate more power at lower wind speeds, while high-speed turbines have higher cut-out speeds around 25-30 m/s and are optimized for higher wind speeds (Munguia, 2023).

2.2.3 Biomass

Biomass can be used to generate electricity through various conversion processes, including combustion, gasification, biological digestion, or fermentation (Dimpl, 2010). One approach is to combust biomass directly to produce steam, which can then drive a turbine to generate electricity, similar to conventional thermal power plants (McKendry, 2002). Alternatively, biomass can be gasified to produce a combustible gas, which can fuel gas engines or turbines for electricity generation (Roman, Barwicki, Hryniewicz, Szadkowska, & Szadkowski, 2021). Biological processes like anaerobic digestion can convert biomass into biogas, which can then be used for electricity production (Dimpl, 2010). The choice of conversion technology depends on factors such as the type of biomass, desired energy form, and overall conversion efficiency (McKendry, 2002). While combustion releases all the available chemical energy, the overall efficiency of converting biomass to electricity can vary from 10-40%, depending on the plant size and technology.

2.3 Energy storage

Energy storage systems for off-grid applications typically involve battery banks, often lithium-ion or lead-acid batteries, to store energy from renewable sources like solar panels and supply power when generation is low (*KIJO Battery*, n.d.). Incorporating hydrogen storage through water electrolysis and fuel cells can enhance system reliability and reduce overall costs by around 30% compared to using only batteries (Noro & Uchiyama, 2021).

2.3.1 Battery Energy Storage System

Batteries are one of the most used energy storage technologies available on the market. The energy is stored in the form of electrochemical energy, in a set of multiple cells, connected in series or in parallel or both, in order to obtain the desired voltage and capacity (Díaz-González, Sumper, Gomis-Bellmunt, & Villafáfila-Robles, 2012). Battery energy storage systems (BESS) store electrical energy in batteries for later use, enabling grid balancing, renewable energy integration, and ancillary services. Common battery types used in BESS include lithium-ion, lead-acid, sodium-sulphur, flow batteries, and vanadium redox batteries, each with its advantages and trade-offs. Lithium-ion batteries offer high energy density and long lifespan, while lead-acid batteries are inexpensive but have lower energy density (FLEXPOWER, 2023).

2.3.2 Hydrogen Energy Storage System

Hydrogen energy storage systems involve converting surplus renewable electricity into hydrogen gas through water electrolysis, storing the hydrogen, and then using it to generate electricity via fuel cells or combustion when needed (Sun et al., 2023). The system typically comprises an electrolyzer for hydrogen production, hydrogen storage tanks, and a fuel cell or turbine for converting the stored hydrogen back into electricity. Proper sizing and operation strategies are crucial for optimizing performance and minimizing costs of the electrolyzer, storage, and conversion components (Miller, Peterson, Randolph, & Ainscough, 2014). These systems enable long-term storage of renewable energy, increase grid flexibility, and provide a means for sectoral integration of energy systems (Melaina, Antonia, & Penev, 2013).

3 Methodology

In this chapter, the methods employed to obtain the results are described, providing a comprehensive overview of the systematic approach adopted for data collection and analysis.

3.1 Description of Proposed System

The schematic diagram in figure (2) depicts an energy-independent system incorporating three key components: Renewable energy sources, hydrogen energy system, and battery energy storage system. The photovoltaic panels harness sunlight and wind turbine harness wind energy to generate electricity, providing a renewable and sustainable energy source. The hydrogen system is responsible for converting surplus electricity from the PV panels/wind turbine into hydrogen through electrolysis, which can be stored and later used to produce electricity through fuel cells or for other applications when solar or wind energy is not available. The battery system complements this setup by storing excess electricity for use during periods of low solar energy production or at night. Together, these components form a comprehensive and reliable energy solution for the client.

3.1.1 Photovoltaic (PV) panel

A typical photovoltaic panel consist of photovoltaic solar cell, front glass, back-sheet, encapsulate material, frame and junction box as shown in the figure(6).

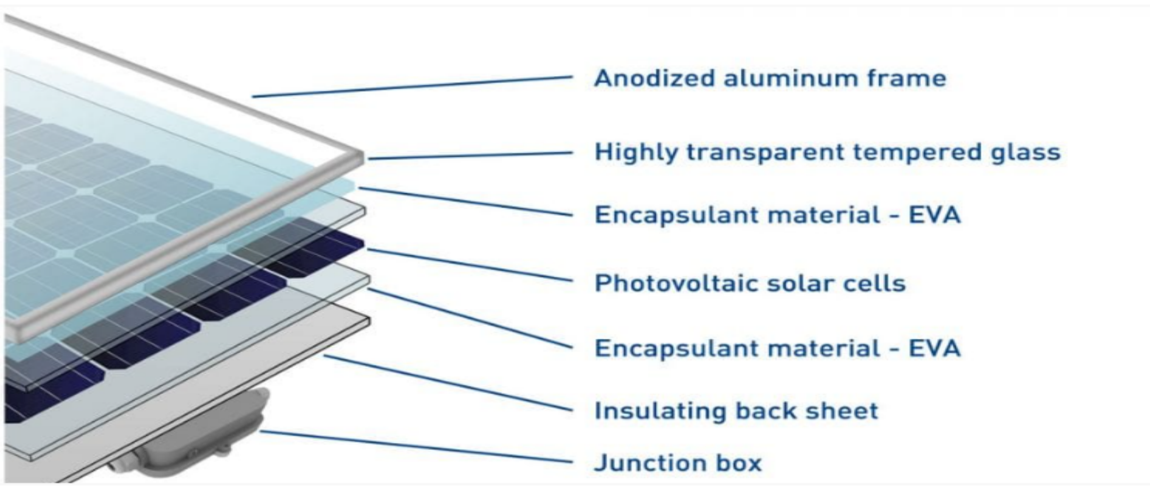

Figure 6: Components of a typical PV module (EcoProgetti, 2021)

There are mainly three different types of solar panels commercially available for solar projects: monocrystalline, polycrystalline and thin film (Lane, n.d.) as shown in figures (7), (8),(9) below.

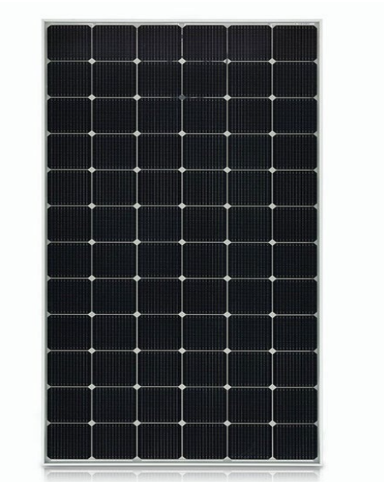

Figure 7: Monocrystalline (Lane, n.d.)

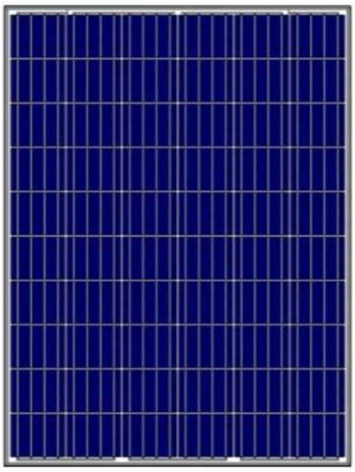

Figure 8: Polycrystalline (Lane, n.d.)

Figure 9: Thin film (Lane, n.d.)

Given that monocrystalline solar panels exhibit the highest efficiency range, typically between 17% and 22%, surpassing polycrystalline (15% to 17%) and thin film (10% to 13%) panels (Lane, n.d.), this project has chosen monocrystalline panels for study. The photovoltaic cell is the major component of the PV module that converts the sunlight into electricity. The number of cells in a solar panel can vary from 36 cells to 144 cells. Generally for rooftop installations 60-cell or 72-cell panels are used. The project is adopting 60-cell half-cut to 120 cells solar panel due to its potential to achieve large wattages in low cost. (Thoubboron, 2018). **Assumptions for modelling of the PV panel**.

- The orientation of solar panel is at 30° slope facing south.
- The PV panel operates with the maximum power point tracking system.

Photovoltaic panel model.
The equivalent circuit of a PV cell consist of a current source, a diode, series resistance (R_s) and shunt resistance (R_{sh}) is shown in figure (10).

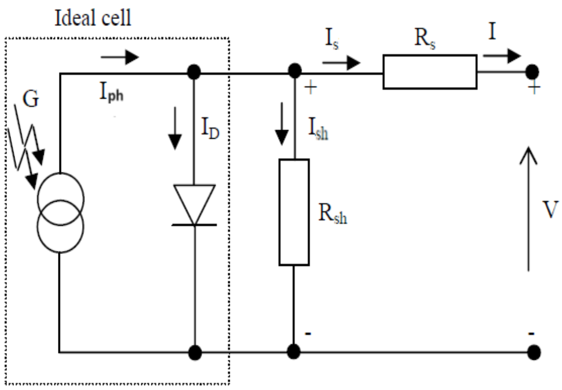

Figure 10: PV cell equivalent circuit (Ramos Hernanz et al., 2010)

The current produced by a single cell is given by equations 1 and 2 (Ramos Hernanz et al., 2010).

$$I = I_{ph} - I_D - I_{sh} \tag{1}$$

$$I = I_{ph} - I_s \left[\exp\left(\frac{q(V + IR_s)}{nkT_c} \right) - 1 \right] - \frac{V + IR_s}{R_{sh}} \tag{2}$$

The cell temperature (T_c) depends upon the ambient temperature and solar irradiation as given by (Tian, Mancilla-David, Ellis, Muljadi, & Jenkins, 2012).

$$T_c = T_{amb} + (NOCT - 20°C)\frac{G}{G_{NOCT}} \tag{3}$$

The generating power of the PV model is given by equation (4) (Hassan, Jaszczur, & Przenzak, 2017), (B. Li, 2018a)

$$P_{PV} = N_{PV} f_{PV} P_{STC} \frac{G}{G_{STC}} \left(1 - \alpha_p \left(T_c - T_{c,STC}\right)\right) \tag{4}$$

3.1.2 Wind Turbine

A wind turbine consists of a rotor mounted on a nacelle, which sits at the top of the tower. The rotor has two or more blades that are mechanically connected to an electric generator. A gearbox within the turbine assembly converts the slower rotational speeds of the rotor into higher speed as needed by the electric generator(Manyonge, Manyala, Onyango, & Shichika, 2012). The components of the horizontal axis wind turbine is shown in figure (11).

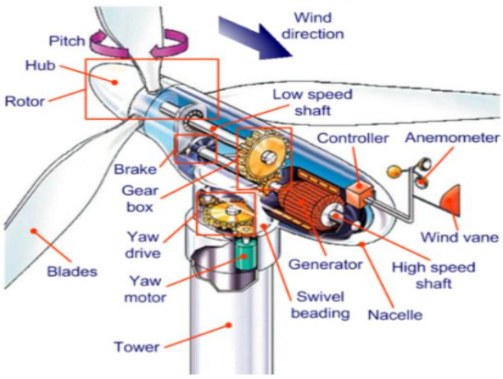

Figure 11: Components of a horizontal axis wind turbine (Christ & Abeykoon, 2015)

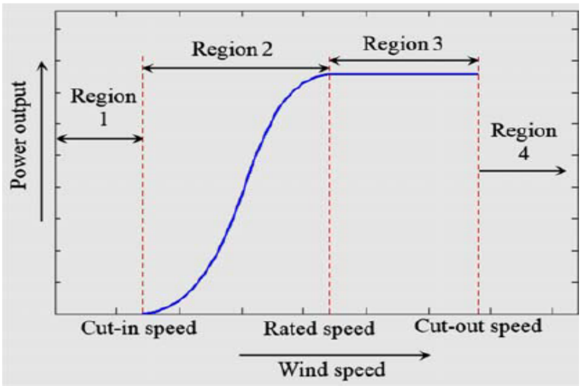

Figure 12: Typical power curve of a wind turbine (Teyabeen et al., 2019)

Wind Turbine model.
A typical power curve of a wind turbine can be seen in figure (12). The power extracted from a wind turbine at any wind speed (v) is given by equation (5) (Abo-Khalil, Alyami, Sayed, & Alhejji, 2019), (Manyonge et al., 2012).

$$P_{WT} = \frac{1}{2}\rho A V_w^3 C_p \tag{5}$$

$$Betz\,limit\,/\,Power\;coefficient\,(C_p) = \frac{(1+\lambda)(1-\lambda^2)}{2} \tag{6}$$

$$\lambda = \frac{blade\,tip\,speed}{wind\,speed} = \frac{V_d}{V_w} \tag{7}$$

$$Blade\,tip\,speed\; = \frac{angular\,speed\,of\,turbine(\omega) \times R}{wind\,speed} \tag{8}$$

The wind speed at different altitudes is given by equation (9) (Abo-Khalil et al., 2019).

$$\frac{V_2}{V_1} = \left(\frac{h_2}{h_1}\right)^{\alpha} \tag{9}$$

Table 1: Wind shear index for various terrain (Abo-Khalil et al., 2019)

Terrain	Empirical Wind Shear Exponent
Smooth, hard ground, lake, or ocean	0.1
Smooth, level, grass-covered	0.14
Tall row crops, low bushes with few trees	0.2
Many trees, occasional buildings	0.24

The data sheet of a wind turbine taken for this project is attached in appendix C. The data sheet contains the power generated at various wind speed. The linear model is adopted for this project where the relationship between the power output at any wind speed can be calculated by linear interpolation as given by equation (10).

$$P_{WT}(V) = P_1 + \frac{P_2 - P_1}{V_2 - V_1}(V - V_1) \tag{10}$$

3.1.3 Hydrogen Electrolyser

Alkaline and PEM (Proton Exchange Membrane) electrolyser technologies are currently commercially available on the market, whereas SOEC (solid oxide electrolyzer cell) and anion exchange membrane technologies are in the process of advancing and maturing (Iea, n.d.). So, this project is adopting the alkaline electrolyser based on its superiority in life time and hydrogen production rate in comparison to PEM electrolyser.

Table 2: Comparison of specifications between PEM and Alkaline Electrolyser

Adopted from (El-Shafie, Kambara, & Hayakawa, 2019)

Specifications	**Alkaline Electrolyser**	**PEM Electrolyser**
Cell temperature (°C)	60 - 80	50 - 80
Cell pressure (bar)	<30	<30
Current density (A/cm^2)	0.2 - 0.4	0.6 - 2.0
Cell voltage (V)	1.8 - 2.4	1.8 - 2.2
Power density (W/cm^2)	Up to 1.0	Up to 4.4
Voltage efficiency (%)	62 - 82	67 - 82
Specific system energy consumption (kWh/Nm^2)	4.5 - 7.0	4.5 - 7.5
Partial load range (%)	20 - 40	0 - 10
Cell area (m^2)	<4	<300
Hydrogen production (Nm^2/hr)	<760	<30
Stack lifetime (hr)	<90,000	<20,000
System lifetime (yr)	20 - 30	10-20
Hydrogen purity (%)	>99.8	99.999
Cold start-up time (min)	15	<15

In an alkaline electrolyzer, electrical energy serves as the driving force for chemical reactions. Water molecules (H_2O) can be split into hydrogen (H_2) and oxygen (O_2) gas via an electrochemical process involving the passage of direct current through electrodes. Typically, the electrolyte used is a potassium hydroxide (KOH) solution, usually containing 20 to 40% by weight, which enhances the ionic conductivity required for the electrolysis process (De Silva & Middleton, 2017). Figure (13) below shows the overall working mechanism of alkaline electrolyser. The electrochemical reaction that takes place in the alkaline electrolyser that splits water into hydrogen (H_2) and oxygen (O_2) can be represented as follows:

$$Cathode \implies 2H_2O + 2e^- \rightarrow 2OH^- + H_2 \tag{11}$$

$$Anode \implies 2OH^- \rightarrow H_2O + 2e^- + \frac{1}{2}O_2 \tag{12}$$

$$Total \implies 2H_2O \rightarrow H_2 + \frac{1}{2}O_2 + H_2O \tag{13}$$

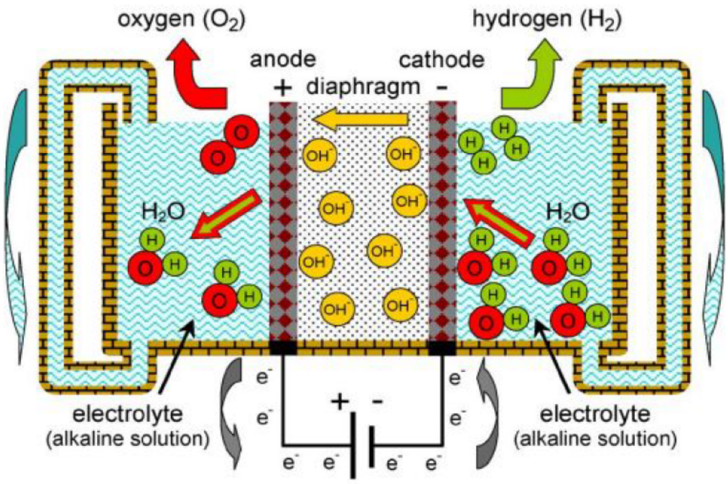

Figure 13: Working principle of alkaline electrolyser (De Silva & Middleton, 2017)

Assumptions for Hydrogen Electrolyser model

The electrolyser system consist of many cells connected in series as per the desired requirement of hydrogen production. The model for this project consist of following assumptions:

- The connected cells in series is completely identical in specification and hydrogen production rate is same for individual cells.
- The electrolyser temperature control system is robust and operates at the constant temperature of 80°C.

Hydrogen Electrolyser model

The I-V characteristics curve (Polarization curve) of a typical alkaline electrolyser can be seen in figure (14) anf figure (15). The electrolyser cell voltage (V_{cell}) is increased from reversible voltage (V_{rev}) due to the losses of irreversible overvoltages as shown in figure (15). The electrolyser cell voltage is sum of reversible voltage and other irreversible voltages as given by equation (14) (De Silva & Middleton, 2017).

$$V_{cell} = V_{rev} + V_{ohm} + V_{act} + V_{con} \tag{14}$$

$$Reversible \quad voltage\,(V_{rev}) = \frac{\Delta G}{2F} = \frac{237.2 \times 10^3}{2 \times 96485} = 1.229V \tag{15}$$

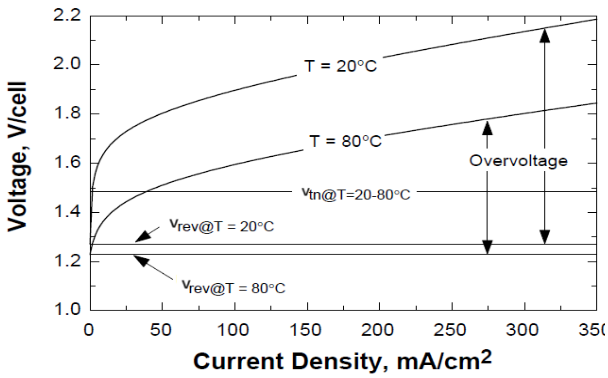

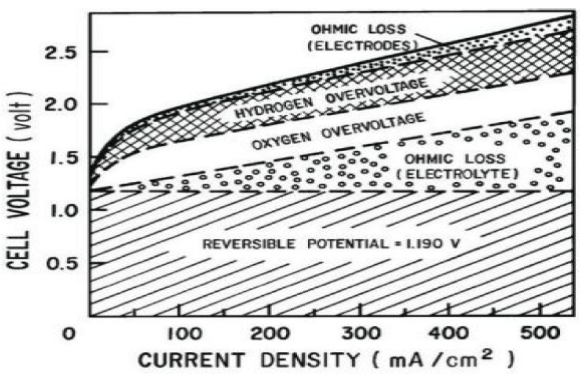

Figure 14: Typical I-V characteristics of a alkaline electrolyser cell at temperatures 20°C and 80°C. *Adopted from(Øystein Ulleberg, 2003)*

Figure 15: I-V characteristics and cell voltages distribution *(De Silva & Middleton, 2017)*

The overvoltage due to ohmic losses are produced by the resistance of electron flow by the components of cell such as electrodes, diaphragm and is given by equation (16) (De Silva & Middleton, 2017) and (Øystein Ulleberg, 2003).

$$Ohmic \quad overvoltage\,(V_{ohm}) = \frac{r_1 + r_2 T}{A} I \tag{16}$$

The activation overvoltage (V_{act}) is the amount of energy required to overcome the electric charge transfer between chemical and electrodes and is given by equation (17) (De Silva & Middleton, 2017) and (Øystein Ulleberg, 2003).

$$Activation \quad overvoltage\,(V_{act}) = s \log\left(\frac{t_1 + \frac{t_2}{T} + \frac{t_3}{T^2}}{A} I + 1\right) \tag{17}$$

The concentration overvoltage (V_{conc}) is caused by the mass transport and in alkaline electrolyser V_{con} is very lower than V_{ohm} and V_{act} and is neglected (De Silva & Middleton, 2017).
Hence final equation for Voltage of single cell (V_{cell}) can be written as:

$$V_{cell} = V_{rev} + \frac{r_1 + r_2 T}{A} I + s \log\left(\frac{t_1 + \frac{t_2}{T} + \frac{t_3}{T^2}}{A} I + 1\right) \tag{18}$$

The total hydrogen production rate in an electrolyser of ($N_{ele-cell}$) numbers of cells connected in series is given by equation 19 (Øystein Ulleberg, 2003).

$$\dot{n}_{H_2} = \eta_F \frac{N_{ele-cell} I}{2F}\,[mol/sec] \;=\; \eta_F \frac{N_{ele-cell} I}{2F}\, 2.016 \times 10^{-3}\,[kg/sec] \tag{19}$$

The Faraday efficiency (η_F) is the ratio of actual hydrogen production and theoretical hydrogen production in the electrolyser. The Faraday efficiency is given by the equation 20 (Øystein Ulleberg, 2003).

$$\eta_F \;=\; \frac{(I/A)^2}{f_1 + (I/A)^2} f_2 \tag{20}$$

The water consumption and oxygen production rates in *[mol/sec]* can be found by equation 21.

$$\dot{n}_{H_2O} \;=\; \dot{n}_{H_2} \;=\; 2\dot{n}_{O_2} \tag{21}$$

3.1.4 Hydrogen Storage and compressor system

Hydrogen produced by electrolyser is first stored at the low pressure buffer storage vessel which is later compressed and sent to the high pressure tank for long term storage. Since, the long term hydrogen storage pressure is kept 345 bar, type III storage tank is sufficient for the project. Type III tank is made of a thick metallic liner hoop wrapped with a fiber-resin composite as shown in figure 16 and 17.
The compressor for this project is taken as a centrifugal compressor of efficiency 85% as shown in figure 18.

Figure 16: Type III storage tank *(Cylinders, 2024)*

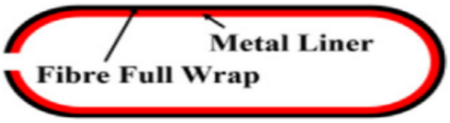

Figure 17: Schematic diagram of type III storage tank *(Cheng et al., 2024)*

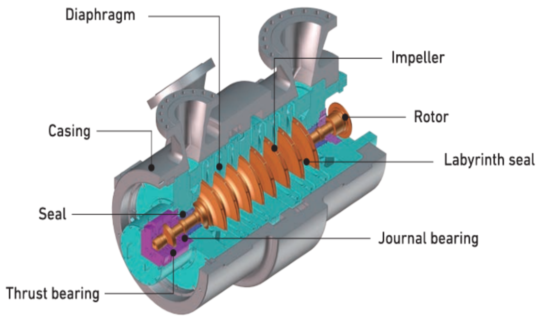

Figure 18: Centrifugal compressor for hydrogen gas compression *(*mitsubushi heavy indrustries group, *n.d.)*

Assumptions for modelling of Hydrogen storage and compressor system

Following assumptions are made for modelling of the hydrogen compression and storage system.

- The hydrogen flow rate from buffer tank to compressor is equal the flow rate coming out of the electrolyser.
- The gas behaves as the ideal gas and the temperature of the gas in the tank is constant.
- Maximum allowable pressure in the hydrogen storage is 345 bar.
- The gas temperature at inlet of the compressor is at ambientc temperature.
- The compression by the centrifugal compression is isentropic compression.

Hydrogen energy storage system model.

The power consumed by the compressor during compression of hydrogen from buffer tank to long term storage tank is given by equation (22) (J. Li et al., 2023a).

$$P_{comp} = \dot{n}_{H_2} C_{pH_2} \frac{T_{in}}{\eta_{comp}} \left[\left(\frac{P_{out}}{P_{in}} \right)^{\frac{k-1}{k}} - 1 \right] \tag{22}$$

The internal pressure of hydrogen can be calculated from the ideal gas law as given by equation(23).

$$P_{tank} = \frac{n_{H_2} R T_{tank}}{V_{tank}} \tag{23}$$

$$n_{H_2} = \int_0^t (\dot{n}_{H_2,in} - \dot{n}_{H_2,out})\, dt \tag{24}$$

$\dot{n}_{H_2,in}$ and $\dot{n}_{H_2,out}$ is the rate of hydrogen flow inside the tank and out of the tank respectively.

3.1.5 Hydrogen Fuel cell system

The proton exchange membrane fuel cell (PEMFC) stands out as the most promising fuel cell type due to its superior efficiency, quick startup capability and widespread commercial availability, as demonstrated in table (3).

Table 3: Comparison of specifications between different types of hydrogen fuel cells (Energy.gov, n.d.)

Fuel Cell Type	Common Electrolyte	Operating Temperature	Typical Stack Size	Electrical Efficiency (LHV)	Applications	Advantages	Challenges
Polymer Electrolyte Membrane (PEM)	Perfluorosulfonic acid	<120°C	<1 kW - 100 kW	60% direct H_2;[i] 40% reformed fuel[ii]	• Backup power • Portable power • Distributed generation • Transportation • Specialty vehicles	• Solid electrolyte reduces corrosion & electrolyte management problems • Low temperature • Quick start-up and load following	• Expensive catalysts • Sensitive to fuel impurities
Alkaline (AFC)	Aqueous potassium hydroxide soaked in a porous matrix, or alkaline polymer membrane	<100°C	1 - 100 kW	60%[iii]	• Military • Space • Backup power • Transportation	• Wider range of stable materials allows lower cost components • Low temperature • Quick start-up	• Sensitive to CO_2 in fuel and air • Electrolyte management (aqueous) • Electrolyte conductivity (polymer)
Phosphoric Acid (PAFC)	Phosphoric acid soaked in a porous matrix or imbibed in a polymer membrane	150 - 200°C	5 - 400 kW, 100 kW module (liquid PAFC); <10 kW (polymer membrane)	40%[iv]	• Distributed generation	• Suitable for CHP • Increased tolerance to fuel impurities	• Expensive catalysts • Long start-up time • Sulfur sensitivity
Molten Carbonate (MCFC)	Molten lithium, sodium, and/or potassium carbonates, soaked in a porous matrix	600 - 700°C	300 kW - 3 MW, 300 kW module	50%[v]	• Electric utility • Distributed generation	• High efficiency • Fuel flexibility • Suitable for CHP • Hybrid/gas turbine cycle	• High temperature corrosion and breakdown of cell components • Long start-up time • Low power density
Solid Oxide (SOFC)	Yttria stabilized zirconia	500 - 1000°C	1 kW - 2 MW	60%[vi]	• Auxiliary power • Electric utility • Distributed generation	• High efficiency • Fuel flexibility • Solid electrolyte • Suitable for CHP • Hybrid/gas turbine cycle	• High temperature corrosion and breakdown of cell components • Long start-up time • Limited number of shutdowns

PEM fuel cell consist of an electrolytic membrane, catalyst layer and gas diffusion layer sandwiched between two electrodes as shown in figure 19. The electrolyte membrane has a property that allows positive ions (H^+) to pass through while blocking electrons. Hydrogen gas passes over anode and with the help of a catalyst, separates into electrons and hydrogen protons. The protons flow to the cathode, through the membrane while the electrons flow through an external circuit, thus creating electricity. The hydrogen protons and electrons combine with oxygen at cathode and produce water.

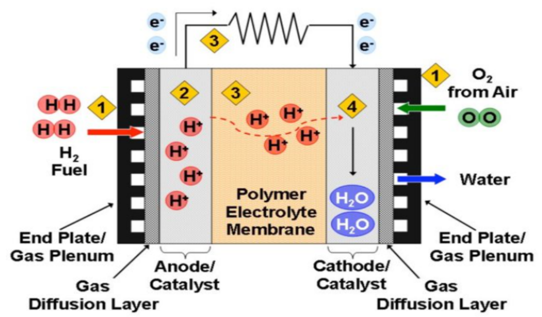

Figure 19: Schematic diagram of a PEM fuel cell (Badami et al., n.d.)

$$At\,anode \implies 2H_2 \rightarrow 4H^+ + 4e^- \quad (25)$$
$$At\,cathode \implies O_2 + 4H^+ \rightarrow 2H_2O \quad (26)$$
$$Overall\ Rx^n \implies 2H_2 + O_2 \rightarrow 2H_2O \quad (27)$$

Assumptions for Modelling of Fuel cell

- The distribution of humidity and temperature inside the fuel cell is uniform.
- Reaction gases obey the law of ideal gases.
- Individual fuel cells are identical and multiple single fuel cells are connected in series to form a stack.
- The temperatures of fuel cell stack is constant.
- The internal resistance of the fuel cell is constant.

Proton Exchange Membrane Fuel cell (PEMFC) Model.
The equivalent electrical circuit and steady state I-V characteristics of a typical fuel cell can be seen in figure (20) and (21) respectively.

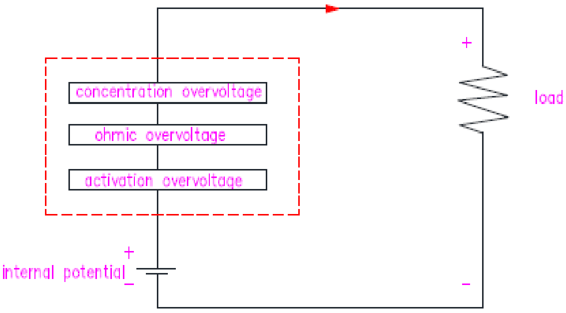

Figure 20: Equivalent electrical circuit of a PEM fuel cell (Zhu et al., 2020)

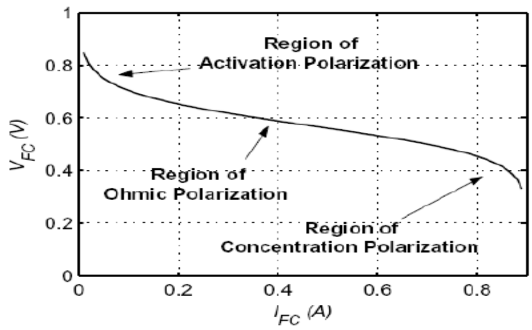

Figure 21: Typical I-V characteristics of a PEM fuel cell (Ural Bayrak & Gençoğlu, 2010)

Due to the irreversible potential also called as overpotential losses the actual voltage output of a fuel cell is less than the theoretical voltage. The three main overpotential that is generated in fuel cell are: 1) Ohmic overpotential (V_{ohm}) 2) Activation overpotential (V_{act}) 3) Concentration overpotential (V_{conc}). The output voltage of PEM fuel cell is given by the following equations (Zhu et al., 2020).

$$V_{cell} = E_{nernst} - V_{act} - V_{ohm} - V_{conc} \tag{28}$$

$$E_{nernst} = 1.229 - 0.85 \times 10^{-3}(T - 298.15) + 4.31 \times 10^{-5}T\left[\ln(P_{H_2}) + \frac{1}{2}\ln(P_{O_2})\right] \tag{29}$$

$$V_{act} = -[\zeta_1 + \zeta_2 T + \zeta_3 T\ln(C_{O_2}) + \zeta_4 T\ln(I_{FC})] \tag{30}$$

$$\zeta_1 = 0.948,\ \zeta_2 = 0.00286 + 0.002\ln(A) + 4.3 \times 10^{-5}\ln(C_{H_2}),\ \zeta_3 = 7.6 \times 10^{-5},\ \zeta_4 = -1.93 \times 10^{-4} \tag{31}$$

$$V_{ohmic} = I_{FC}\,(R_M + R_C) \tag{32}$$

$$R_M = \frac{\rho_M l}{A} \quad Where \quad \rho_M = \frac{181.6\left[1 + 0.03\left(\frac{I_{FC}}{A}\right) + 0.062\left(\frac{T}{303}\right)^2\left(\frac{I_{FC}}{A}\right)^{2.5}\right]}{\left[\psi - 0.634 - 3\left(\frac{I_{FC}}{A}\right)\right]\exp\left[4.18\left(\frac{T-303}{T}\right)\right]} \tag{33}$$

$$C_{O_2} = \frac{P_{O_2}}{5.08 \times 10^6 \exp^{-\left(\frac{498}{T}\right)}} \quad And \quad C_{H_2} = \frac{P_{H_2}}{9.174 \times 10^7 \exp^{-\left(\frac{77}{T}\right)}} \tag{34}$$

$$V_{conc} = -B\ln\left(1 - \frac{J}{Jmax}\right) \tag{35}$$

PEM fuel cell are connected in series to form a stack so the total voltage of stack is given by:

$$V_{stack} = N_{cell}V_{cell} \tag{36}$$

3.1.6 Battery storage system

Battery storage systems are the electrochemical way of storing the energy. The comparison between different commercially available battery storage by various specifications are shown in table (4) below.

Table 4: Comparison of specifications between different types of Battery (University, 2020)

	NiCd	NiMH	Lead Acid	Li-ion	Li-ion polymer
Gravimetric Energy Density(Wh/kg)	45-80	60-120	30-50	110-160	100-130
Internal Resistance (includes peripheral circuits) in mΩ	100 to 200 6V pack	200 to 300 6V pack	<100 12V pack	150 to 250 7.2V pack	200 to 300 7.2V pack
Cycle Life (to 80% of initial capacity)	1500	300 to 500	200 to 300	500 to 1000	300 to 500
Fast Charge Time	1h typical	2-4h	8-16h	2-4h	2-4h
Overcharge Tolerance	moderate	low	high	very low	low
Self-discharge / Month (room temperature)	20%	30%	5%	10%	~10%
Cell Voltage(nominal)	1.25V	1.25V	2V	3.6V	3.6V
Load Current					
- peak	20C	5C	5C	>2C	>2C
- best result	1C	0.5C or lower	0.2C	1C or lower	1C or lower
Operating Temperature(discharge only)	-40 to 60°C	-20 to 60°C	-20 to 60°C	-20 to 60°C	0 to 60°C
Maintenance Requirement	30 to 60 days	60 to 90 days	3 to 6 months	not req.	not req.
Commercial use since	1950	1990	1970 (sealed lead acid)	1991	1999

The lithium-ion battery is the optimal choice for this project due to its advantages in high energy density and a compact, lightweight design compared to other battery technologies.

Assumptions for Modelling of Battery storage system

- The maximum permissible state of charge (SOC) for battery system is 80% with charging efficiency of 98%.
- The minimum permissible depth of discharge (DOC) for battery system is 80% with discharging efficiency of 97%.
- The battery management system (BMS) is robust enough to control the battery to ensure that its operation stays within the designed limits.

Battery storage system model.
The energy stored in the battery can be measured by state of charge (SOC), which is the ratio of stored energy and the nominal storage capacity of the battery (Serra, Lucariello, Petrollese, & Cau, 2020).

$$SOC(t) = \frac{C_{bat}(t)}{C_{nom}} \tag{37}$$

For charging and discharging occurring over time, the state of charge (SOC) at any point of time (t) is given by equation(38) (B. Li, 2018b).

$$SOC(t) = SOC(t-1) + \frac{P_{ch}(t)\eta_{ch}\Delta t}{C_{nom}} - \frac{P_{dis}(t)\eta_{dis}\Delta t}{C_{nom}} \tag{38}$$

3.2 Energy Management System

The energy management strategy for off-grid system proposed in this paper is shown in figure (22). As the logical diagram suggests the user demand are first matched by the renewable energy sources, whereas battery storage are the first energy storage involved to cover the deficit of energy. If the energy storage of battery is insufficient to compensate for user demand , the fuel cell fulfils the deficit. The system is designed optimum enough to always meet the user demand.
On the other side, if the energy production of sources exceeds user demand, battery storage is first charged fully and then hydrogen electrolyser is turned on. The system is carefully balanced to avoid over-designing and surpassing production power.

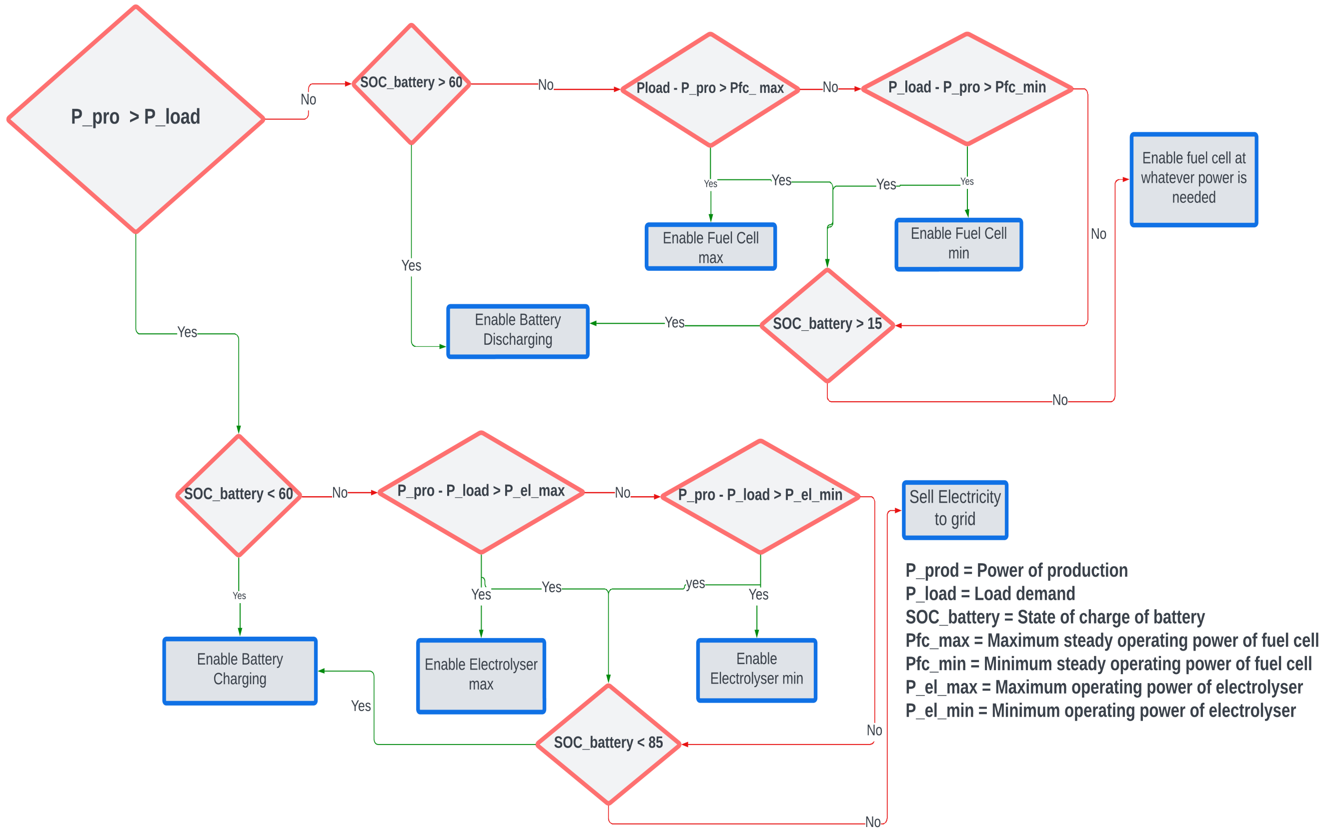

Figure 22: Logic diagram of energy management for the proposed system

3.3 Load Profile of consumer

The houses within the Rosandepolder community exhibit a varied distribution of energy loads. While some houses utilize conventional boilers, others and only few rely on heat pumps. Furthermore, the presence of electric vehicles in some households contributes to higher energy consumption. Additionally, the community displays diversity in cooking methods, with some houses using conventional gas and others using electricity. These variations in electricity usage patterns contribute to the overall diversity in energy consumption within the community.
The yearly energy usage of the 44 houses in Rosandpolder community as provided by community is shown in figure 23 below.

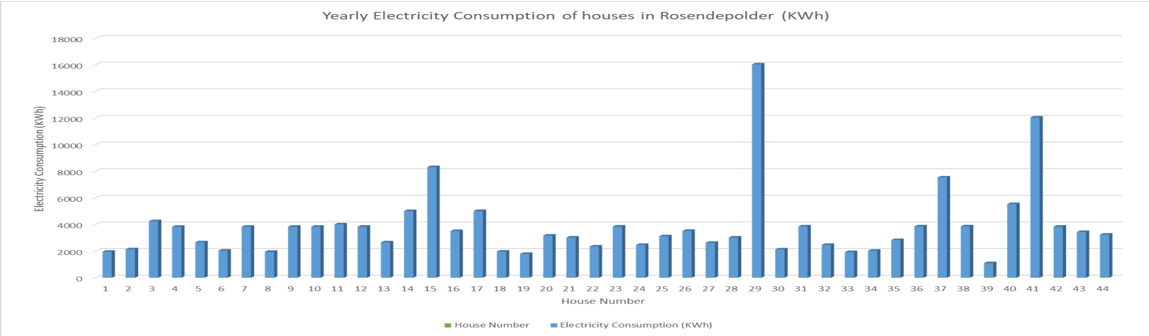

Figure 23: Yearly electricity consumption of houses of Rosandepolder community

Total electricity consumption yearly of the community is compared with the electricity consumption of households in the Netherlands in 2023 as shown in figure 24. On calculating the same consumption weight-age per month monthly electricity consumption of Rosandepolder community is calculated as shown in figure 25.

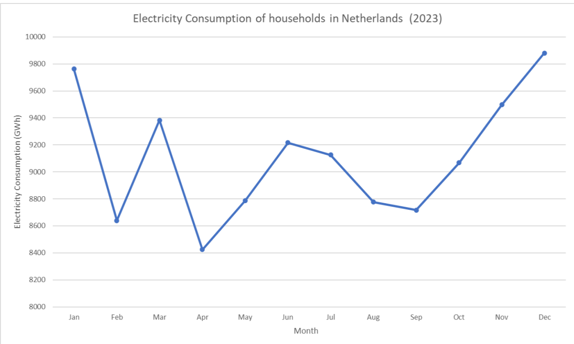

Figure 24: Monthly electricity consumption in the Netherlands in 2023 (*Database - Eurostat*, n.d.)

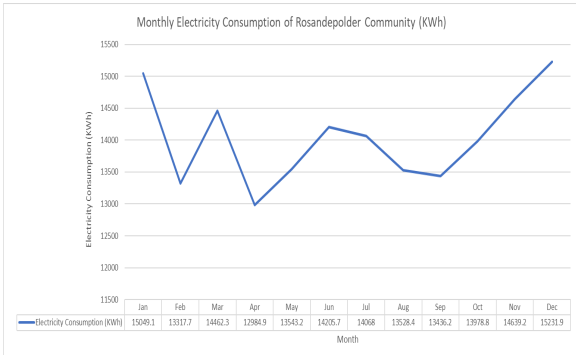

Figure 25: Monthly electricity consumption of Rosandepolder community

Hourly electricity demand of community is calculated by comparing the demand from case study in 2014 in Wageningen, the Netherlands from paper (Azari, 2020).

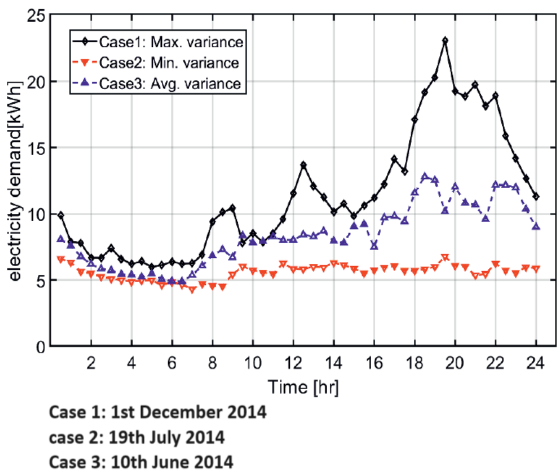

Figure 26: Load profile of consumer in Wageningen, the Netherlands in 2014 (Azari, 2020)

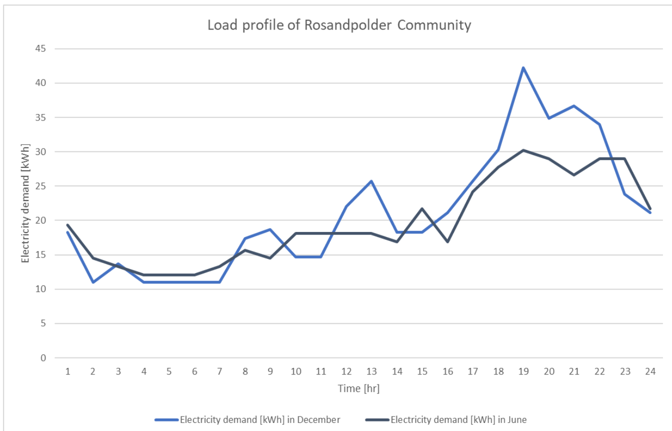

Figure 27: Load profile of Rosandepolder community per hour

3.4 MATLAB Simulink Model

Figure 28 gives an overview of the system created in MATLAB Simulink.

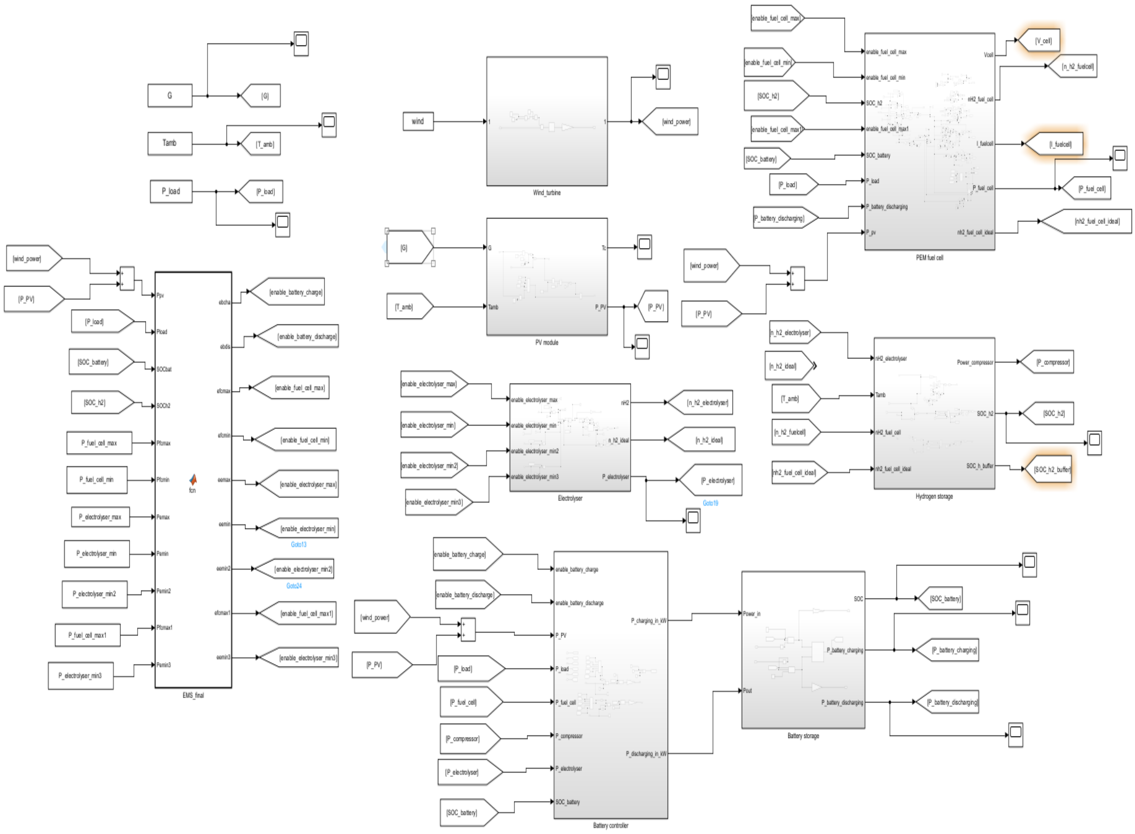

Figure 28: System overview in MATLAB-Simulink

3.5 Simulation Scenarios

To answer the research questions, model created in MATLAB-Simulink is simulated for following three scenario cases:

3.5.1 Scenario 1 : Electricity independent system with PV panel as energy source

This scenario assesses a system that is self-sufficient in electricity, with PV panels as the sole source of power generation. Input parameters of solar irradiation (G) and ambient temperature (T_{amb}) for the entire year in Rosandepolder are obtained from (*pvgis.com*, n.d.), as shown in Figures 49 and 50 and load profile for this scenario is shown in 52 in Appendix D.

3.5.2 Scenario 2 : Electricity independent system with PV panel and wind turbine as energy source

This scenario is applied to assess the system for electricity independence, similar to Scenario 1, with PV panels and a wind turbine as the sources for power generation. Input parameters of solar irradiation (G), ambient temperature (T_{amb}), and wind speed for the entire year in Rosandepolder are obtained from (*pvgis.com*, n.d.), as shown in Figures 49, 50, and 51 and load profile for this scenario is shown in 52 in Appendix D.

3.5.3 Scenario 3 : Energy independent system with PV panel and wind turbine as energy source

This scenario is applied to assess the system with the objective of achieving complete energy independence, including the elimination of gas usage, using PV panels and a wind turbine as the sources for power generation. Input parameters of solar irradiation (G), ambient temperature (T_{amb}), and wind speed for the entire year in Rosandepolder are obtained from (*pvgis.com*, n.d.), as shown in Figures 49, 50, and 51 and load profile for this scenario is shown in 53 in Appendix D.

3.6 Selection of validation method

The complete system model cannot be validated as this is a noble project in itself for community of Rosandepolder. Validation of the model is done by comparing the individual sub-components models simulation result with the results from existing research.

3.7 Economic Assessment

The economic analysis of the entire system is based on the estimation of capital expenditure (CAPEX) and operational expenses (OPEX). CAPEX encompasses the costs associated with establishing the whole system, including the purchase and installation of all necessary components. OPEX refers to the ongoing costs required to operate and maintain the system over its lifetime. To derive accurate estimates, various literatures were reviewed to determine the capital costs of each component within the plant. These costs were then aggregated to calculate the total CAPEX. Similarly, the estimated variable costs for running and maintaining the system were summed to determine the OPEX of the proposed system. This comprehensive economic analysis is crucial for assessing the financial feasibility and long-term sustainability.

Table 5: CAPEX and OPEX of the system components

CAPEX (Capital Expenses)			
Component Name	**Technical Lifetime**	**Investment Costs**	**Source**
PV panel	25	240 €/kW	(J. Li et al., 2023a)
Wind turbine	25	1766 €/kW	(Alonso, Costa, Messagie, & Coosemans, 2024)
Battery(Lithium-ion)	15 years	139 €/KWh	(Spector & McCarthy, 2023)
Electrolyser	15 years	1666 €/KW	(*Electrolyser cost—EHO*, n.d.),(Alonso et al., 2024)
Fuel Cell	15 years	2000 €/KW	(SRO, n.d.)
Hydrogen Storage	25 years	20 €/ltr	(Alonso et al., 2024), quotation (Cylinders, 2024)

OPEX (Operational Expenses)		
Component Name	**Field Operational and Maintenance Costs**	**Source**
PV panel	1% of CAPEX	(Alonso et al., 2024)
Wind turbine	1 % of CAPEX	(Alonso et al., 2024)
Battery (Lithium-ion)	4% of CAPEX	(Alonso et al., 2024)
Electrolyser	42.50 EUR/KW/yr	(*Electrolyser cost—EHO*, n.d.)
Fuel Cell	4% of CAPEX	(Alonso et al., 2024)
Hydrogen Storage	1% of CAPEX	(Alonso et al., 2024)

3.7.1 Net present value

Net present value (NPV) method is generally used to compare the alternative cases and choose the alternative with the greatest positive net present value (Turton, Bailie, Whiting, & Shaeiwitz, 2008). To calculate net present value, cash flows at different period of time during the project's life time is discounted to the present value and initial investment is subtracted from the sum of the project's discounted cash flow as given by equation 39 (Fernando, 2024).

$$NPV = Sum\,of\,all\,discounted\,cash\,flows\;-\;initial\;investment \tag{39}$$

The single cash-flow and uniform series cash flow can be discounted to present worth as given by equation (40) and (41) respectively.

$$Present\,value\;=\;\frac{Cash\,flow}{(1+i)^n}\rightarrow\rightarrow\rightarrow\rightarrow\rightarrow\rightarrow For\,single\,cash\,flow \tag{40}$$

$$Present\,value\;=\;Cash\,flow\,\frac{(1+i)^n-1}{i(1+i)^n}\rightarrow\rightarrow\rightarrow For\,periodic\,(yearly)\,cash\,flow \tag{41}$$

3.7.2 Discounted Payback Period (DPBP)

Payback period is generally calculated to measure the profitability of the project. Payback period can be simple or discounted depending upon whether time value of money is taken into account or not. Discounted payback period is the time required to recover the fixed capital investment provided that calculation is made with all the cash flow discounted back to present value (Turton et al., 2008). Lower the discounted payback period more desirable is the project.

4 Results and Discussion

This chapter presents the validation for each subsystem, followed by the results and discussion. It concludes with the results of the economic analysis of the system configurations.

4.1 Validation of model

Before presenting the simulated results and their discussion, it is essential to validate the effectiveness of the developed model. Since there is no real system installed at the current stage, the validation of the simulated model cannot be achieved by comparing the simulation results with measured inputs and outputs. Therefore, the validation of the entire model is carried out by validating the sub-models using data and results from existing literature or by providing logical explanations of the results.

4.1.1 Photovoltaic (PV) panel

The data sheet of the PV panel adopted for the project is attached in Appendix B. The simulated power output of the PV model at standard test conditions (STC) and normal operating conditions (NOC) is presented in Figure 29.

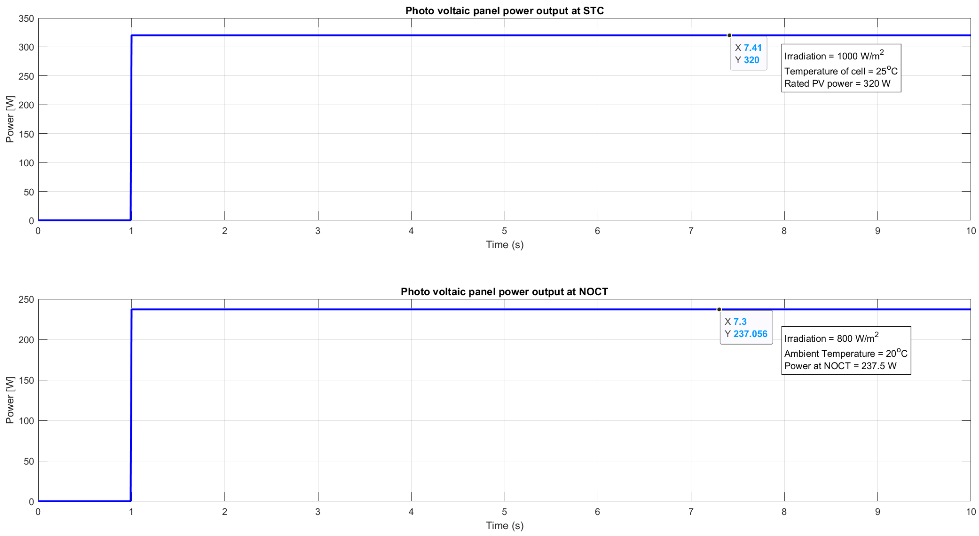

Figure 29: Simulated results of PV panel at STC and NOC

By comparing the simulated results with the data sheet, it can be seen that the power outputs of 320 W at STC and 237.5 W at NOC match exactly, ensuring the accuracy of the PV model.

4.1.2 Electrolyser

To validate the electrolyser model, a literature study (Øystein Ulleberg, 2003) with similar parameters to this project was found and on comparing both the results as displayed in figure 30 and 31 below. The comparison indicates a match between our model and the results from (Øystein Ulleberg, 2003) which contains both measured and simulated data, provides strong evidence of the model's accuracy and validity. The operating pressure is 7 bar and the cell voltage increases with decrease in temperature as expected in both of the figures. The parameters for simulation are provided in appendix A.

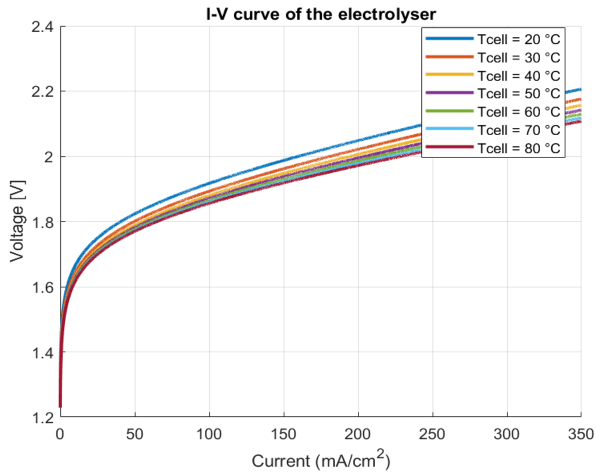

Figure 30: Simulated results I-V curve for electrolyser at temperature 20 to 80 °C

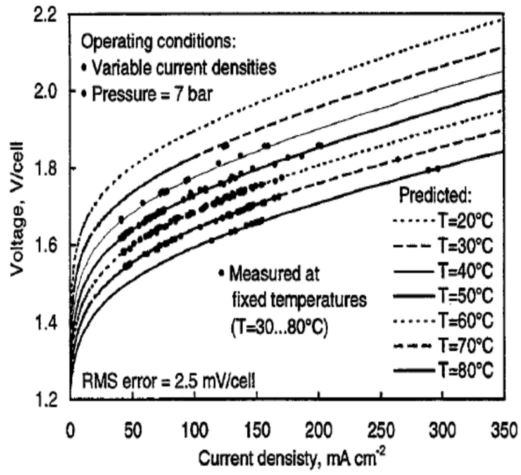

Figure 31: simulated versus measured cell voltage at temperature 20 to 80 °C (Øystein Ulleberg, 2003)

4.1.3 Fuel cell

The fuel cell model is validated by comparing the I-V curve of a 32-cell stack with the results from a study by (Correa et al., 2005) as shown in figures 32 and 33. The paper by (Correa et al., 2005) provides a comparison between manufacturing and simulation results, making it a suitable reference for our validation process. Both figures utilize the same parameters provided in appendix A, with 32 cells considered for simulation in both models. The close match between the voltage at different current densities confirms the validation of our fuel cell model.

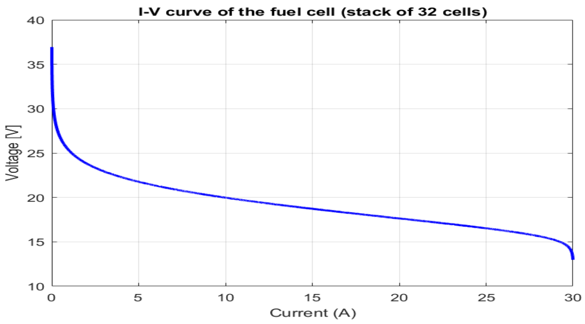

Figure 32: Simulated results I-V curve for fuel cell at temperature 60 °C (333.15 K)

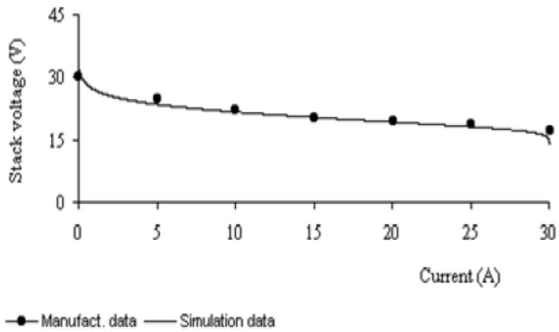

Figure 33: simulated versus manufacturer provided I-V curve at temperature 20 to 80 °C (Correa et al., 2005)

4.1.4 Battery storage system

The battery storage system is validated by logical explanation of the results in a controlled test condition. For this validation process, a capacity of 100 kWh is assigned to the battery. In the first hour, a constant charging power of 50 kW is applied, followed by a constant discharging power of 50 kW in the subsequent hour. The simulation result of the model is illustrated in Figure 34 below. The state of charge (SOC) of the battery storage increases by nearly 50% during the charging mode, as expected. Similarly, during the discharging mode, the SOC decreases by nearly 50%, returning to almost the original state of charge. The difference between the original SOC and the final SOC is occurred due to the influence of charging and discharging efficiencies.

This simulation results demonstrates the expected behaviour of the battery storage system under the specified test conditions. It confirms that the model accurately reflects the charging and discharging dynamics of the battery, validating its effectiveness for use within the project.

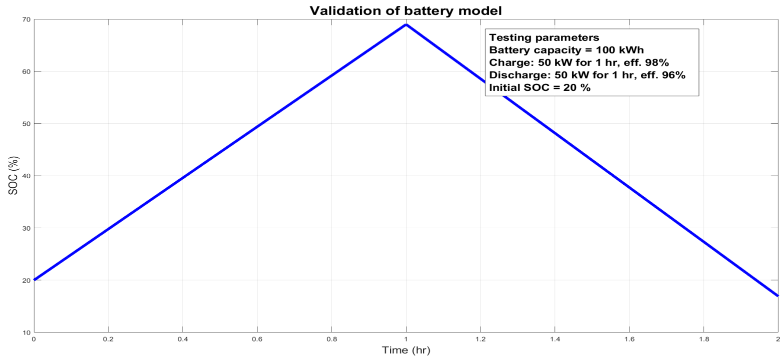

Figure 34: Soc of battery model in a test condition

4.1.5 Hydrogen production system

Hydrogen storage system is the difference in inflow of hydrogen from electrolyser and outflow to the fuel cell. The amount of hydrogen produced in the electrolyser depends upon the Faraday efficiency as given by 20. The Faraday efficiency is validated with the results from (Øystein Ulleberg, 2003) as illustrated in figures 35 and 36. For the operating temperature of 80°C the efficiency is nearly 98% in both of the figure.

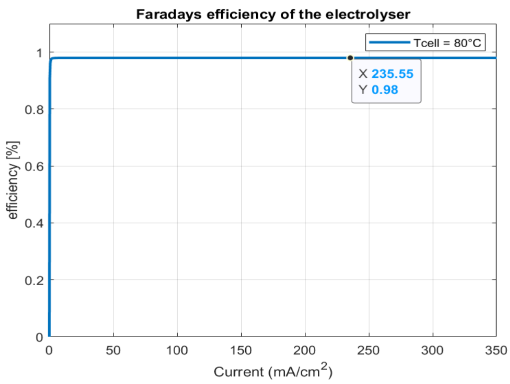

Figure 35: Simulated Faraday efficiency

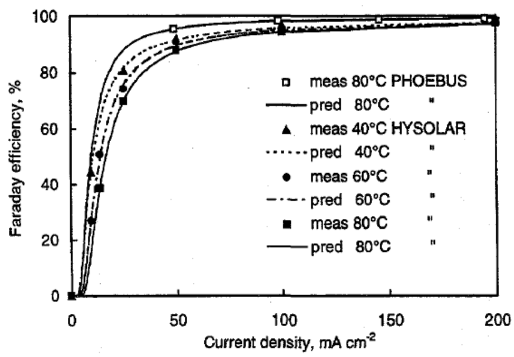

Figure 36: Predicted versus measured Faraday efficiency °C (Øystein Ulleberg, 2003)

4.2 Results and discussion of scenario 1

In this scenario, PV panels serve as the sole energy sources in the energy-independent system. A total capacity of 218 kW of solar panels is utilized for the simulation. The community's total load demand is divided into daily and hourly segments, as detailed in Section 3.3. Through simulations varying the capacities of the electrolyser, fuel cell, battery storage, and hydrogen storage system, the final optimal capacities were determined to be:

1. Electrolyser: 100 kW
2. Fuel Cell: 45 kW
3. Hydrogen Storage Tank: 12,000 litres
4. Battery Pack: 500 kWh

With these system capacities, the total available power consistently meets or exceeds the load demand at all times, as illustrated in Figure 37.

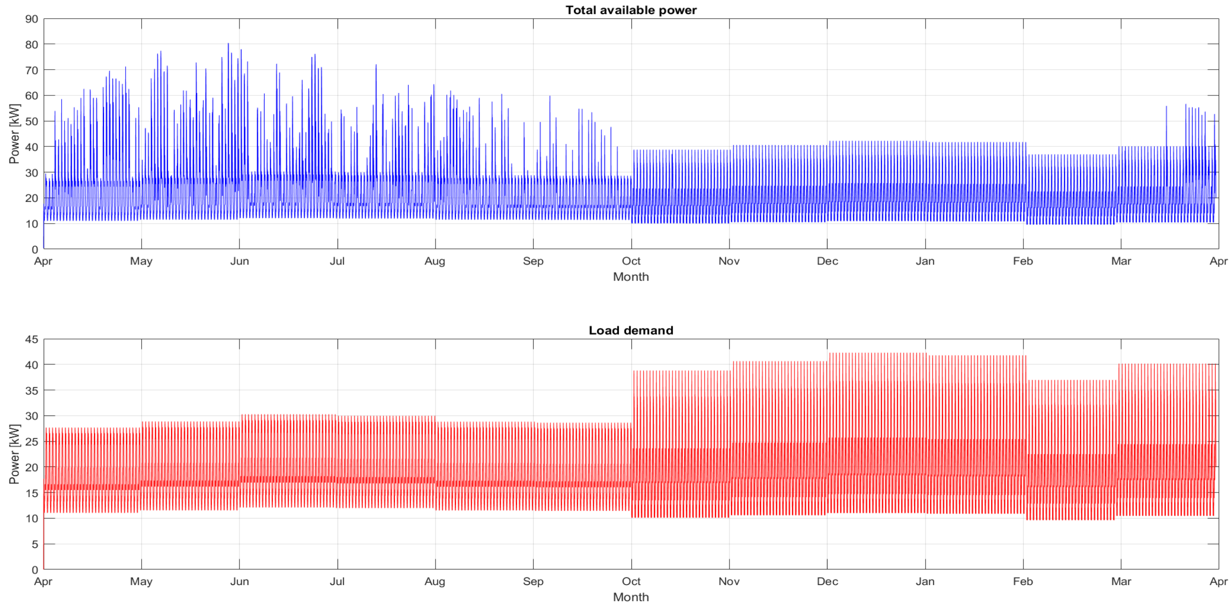

Figure 37: Total available power, load demand - scenario 1

The simulation starts from April as shown in figure 38 where the solar panel is producing in a huge amount till end of September as expected because of the high amount of solar irradiation in summer. Where as, during winter from September to end of March total electricity production from panel is at its low. The excess electricity remaining even after charging the battery and turning to hydrogen, during summer is sent to grid. This is important because if we desire to consume this excess power the system will be unnecessarily so big.

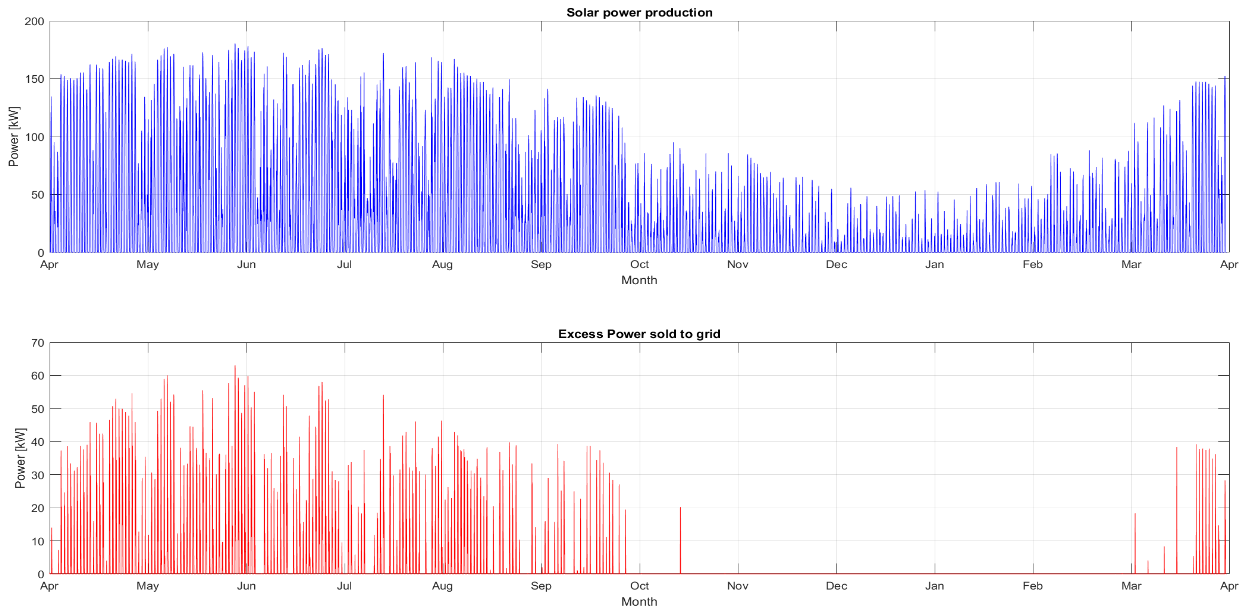

Figure 38: Total power production of solar panel, Excess electricity sold to the grid - scenario 1

The power consumed by the electrolyser and power produced by fuel cell is displayed in figure 39. The power consumption of the electrolyser follows a similar trend to the solar power production, as the excess electricity is converted to hydrogen. Similarly, the fuel cell operates at its maximum capacity during winter when solar power production is low, ensuring that demand is met by running at peak output.
This cycle can be further illustrated from figure 40, where the state of charge (SOC) of hydrogen peaks during the summer and gradually decreases as it is consumed by the fuel cell, which operates at peak power during winter. The battery storage system acts as a fluctuation manager, ensuring that the fuel cell and electrolyser can run at steady power levels. The primary purpose of the battery is to manage fluctuations, whether in charging or discharging mode, to maintain smooth operation of the overall system.

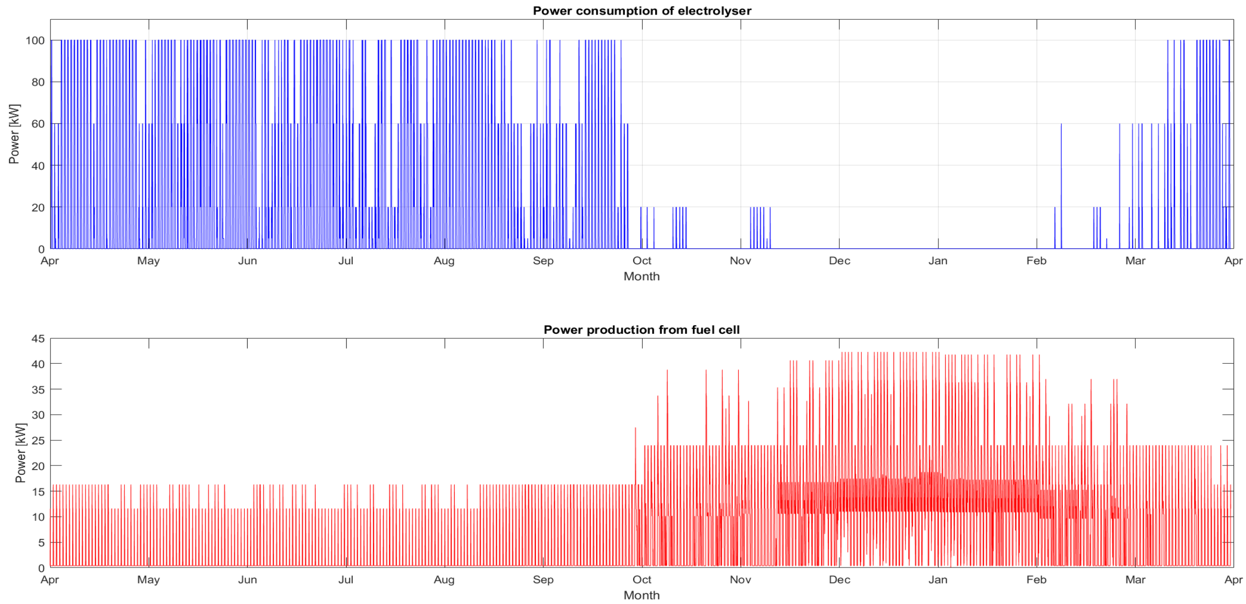

Figure 39: Total power consumption of electrolyser, Power production of fuel cell - scenario 1

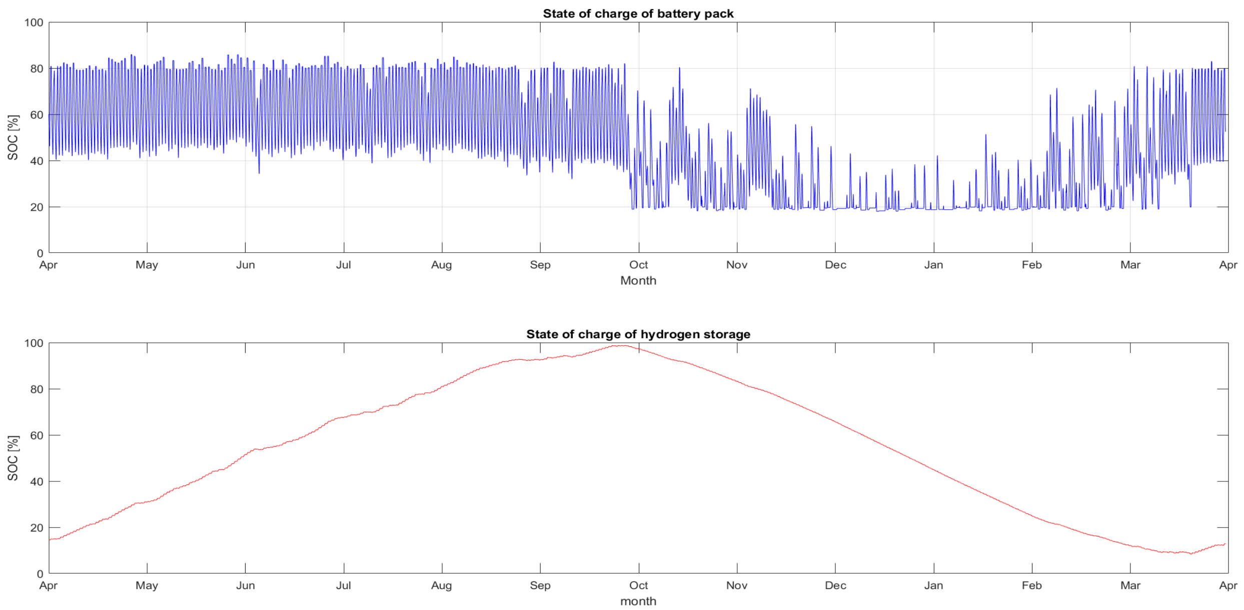

Figure 40: SOC of battery, SOC of hydrogen - scenario 1

4.3 Results and discussion of scenario 2

In this scenario, photovoltaic (PV) panels and a wind turbine are combined to serve as the energy sources. The load demand remains the same as in Scenario 1, where the focus was on achieving electricity independence for the client. The addition of the wind turbine allows for power generation during the winter months, which is crucial for balancing production and supply demands while reducing the size of the sub-components.
Here, a 177 kW capacity solar panel system is connected with a 60 kW wind turbine. Through simulation, the necessary capacities for the electrolyser, fuel cell, storage, and battery bank to ensure electricity independence from the grid were determined as follows:

1. Electrolyser: 60 kW
2. Fuel Cell: 45 kW
3. Hydrogen Storage Tank: 8,000 litres
4. Battery Pack: 300 kWh

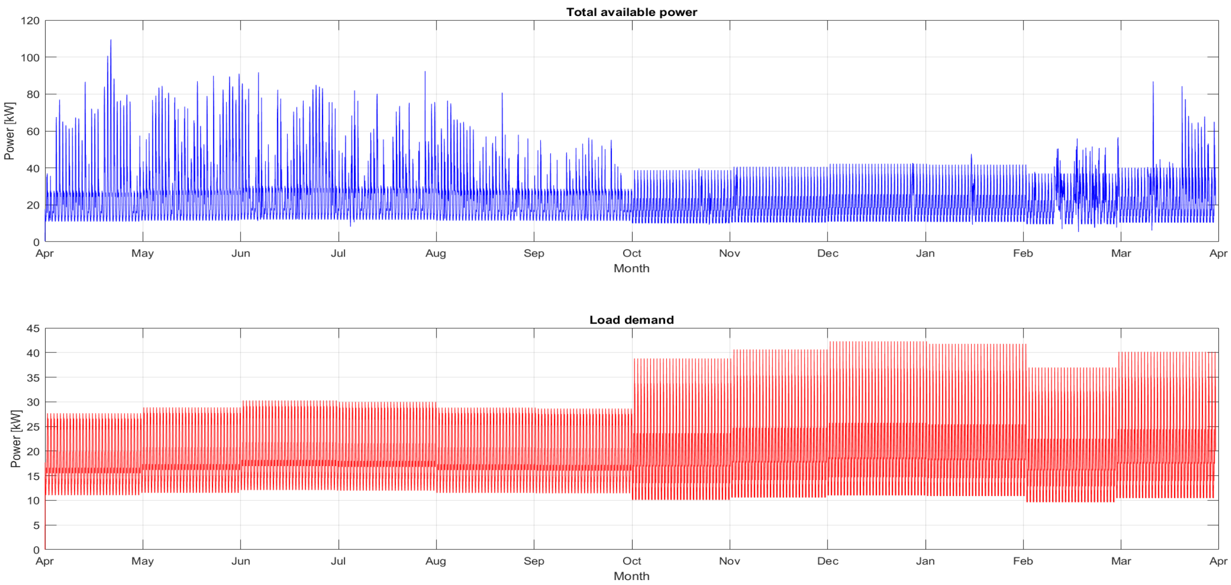

Figure 41: Total available power, Total load demand - scenario 2

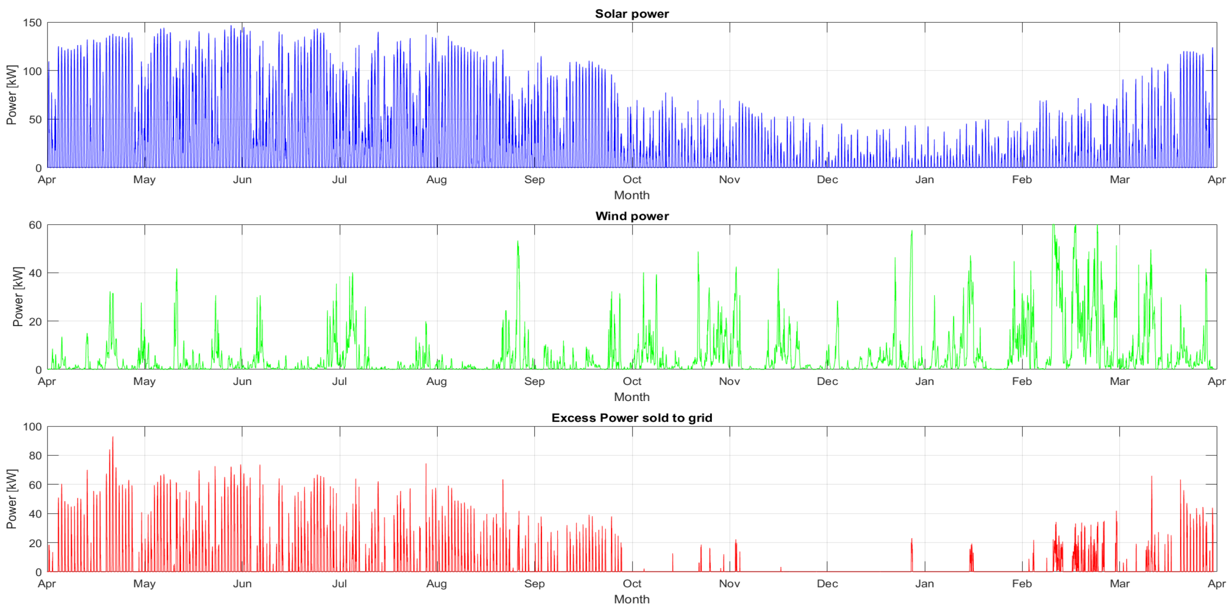

Figure 42: Total power production of solar panel, Excess electricity sold to the grid - scenario 2

The average wind velocity at the location is 3.9 m/s at a height of 25 meters, which is generally very low for wind turbines. Most of the time, the wind speed is below the cut-in speed specified in the data-sheet attached in Appendix C. Consequently, for the 60 kW wind turbine, the power output, as shown in Figure 42, is low, indicating that the wind turbine is not operating at its full potential. However, due to the distributed electricity production throughout the year because of wind turbine, the required capacity for the storage system and the electrolyser was reduced by nearly 40% from that of scenario 1 as illustrated in Figures 43 and 44

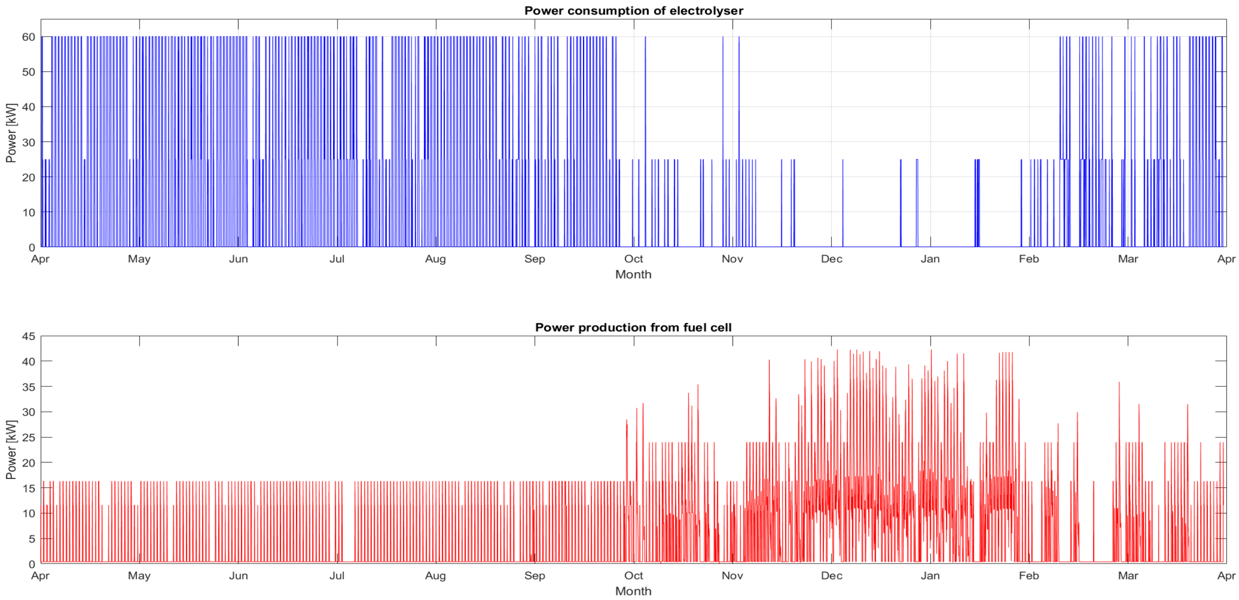

Figure 43: Total power consumption of electrolyser, Power production of fuel cell - scenario 2

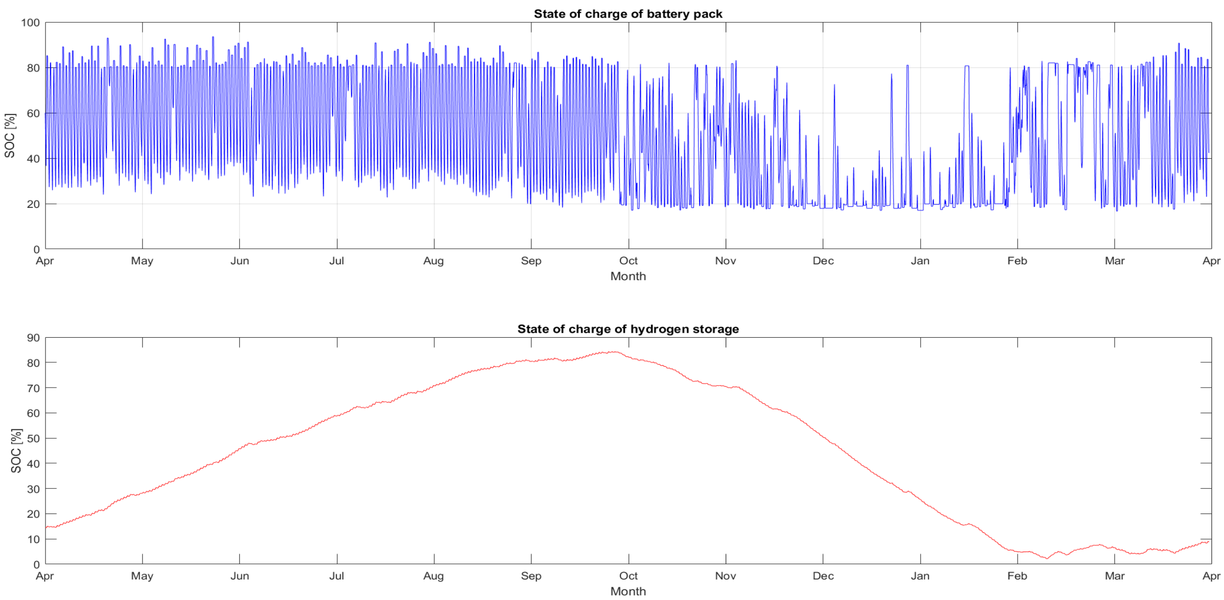

Figure 44: SOC of battery, SOC of hydrogen - scenario 2

4.4 Results and discussion of scenario 3

In this scenario, photovoltaic panel (PV) of capacity 280 kW is combined with 60 kW wind turbine as the energy source. The load profile for this scenario also incorporates the energy for heating replacing the conventional gas by heat pump. On simulation, optimal sizes of electrolyser, fuel cell, battery pack and hydrogen storage tank found to achieve energy independence are as follows:

1. Electrolyser: 140 kW
2. Fuel Cell: 70 kW
3. Hydrogen Storage Tank: 26,000 litres
4. Battery Pack: 700 kWh

The load demand for summer is similar in Scenario 1 and Scenario 2. However, during the winter, the load demand increases significantly due to the additional electricity required for heat pumps. This is illustrated by the load demand in Scenario 3, as shown in Figure 45. The increased demand during winter necessitates a higher capacity for energy storage, which is expected. Although the energy produced by the wind turbine is not at its full capacity due to the low distribution of wind at the location, it helps balance supply and demand during winter. This contribution ultimately reduces the overall size of the required components, as observed in Scenario 2.

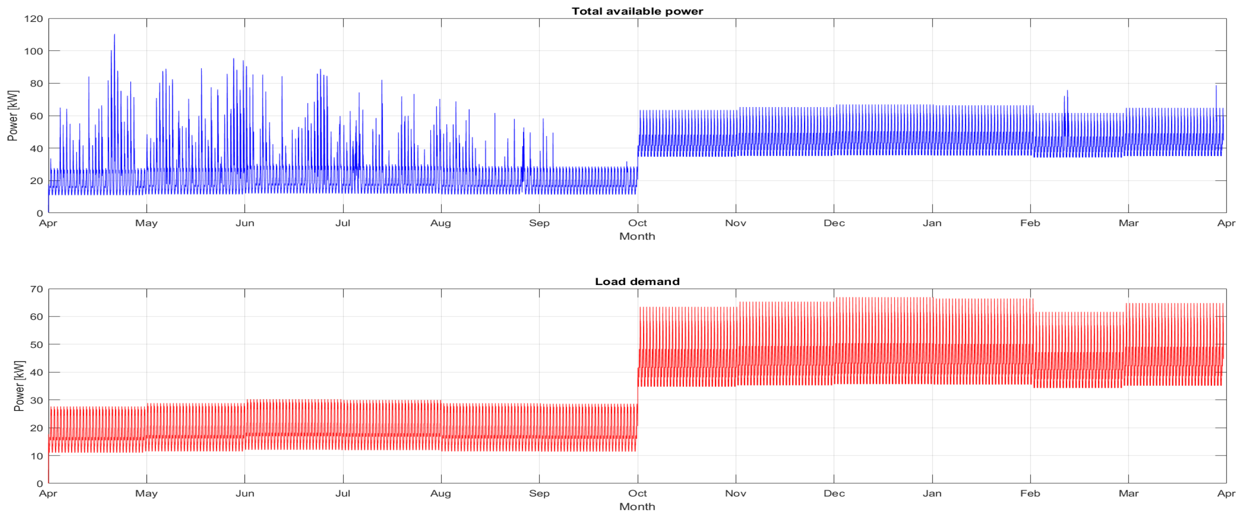

Figure 45: Total available power, Total load demand - scenario 3

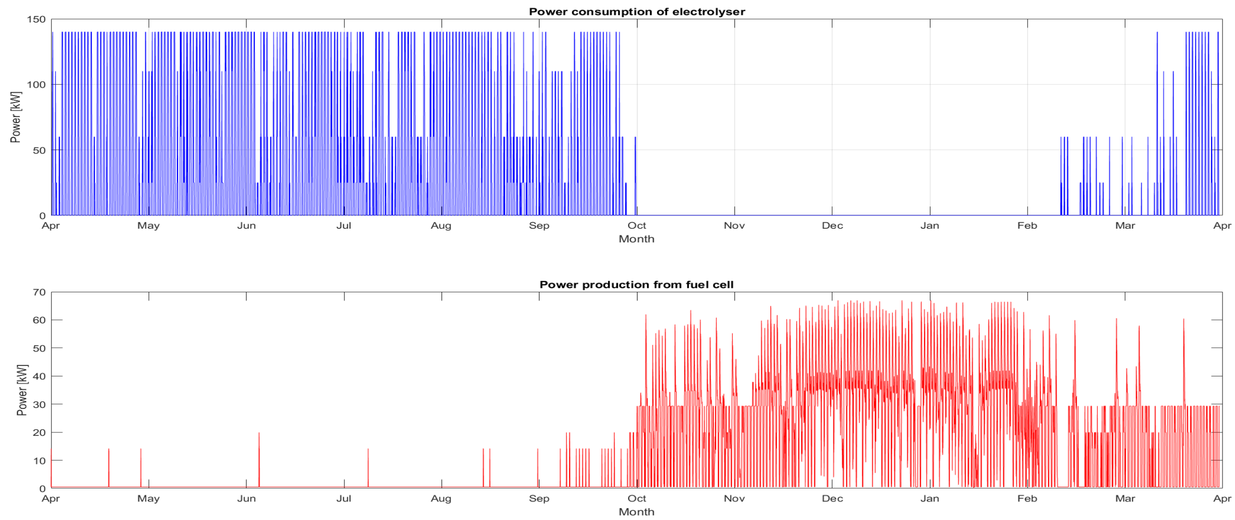

Figure 46: Total power consumption of electrolyser, Power production of fuel cell - scenario 3

The electrolyser produces hydrogen during the summer when there is an excess of electricity, while the fuel cell is mostly activated during the winter. The State of Charge (SOC) of the battery fluctuates on a daily basis to balance the daily variations in supply and demand. In contrast, the SOC of hydrogen increases during the summer and decreases in the winter, as shown in Figure 48.

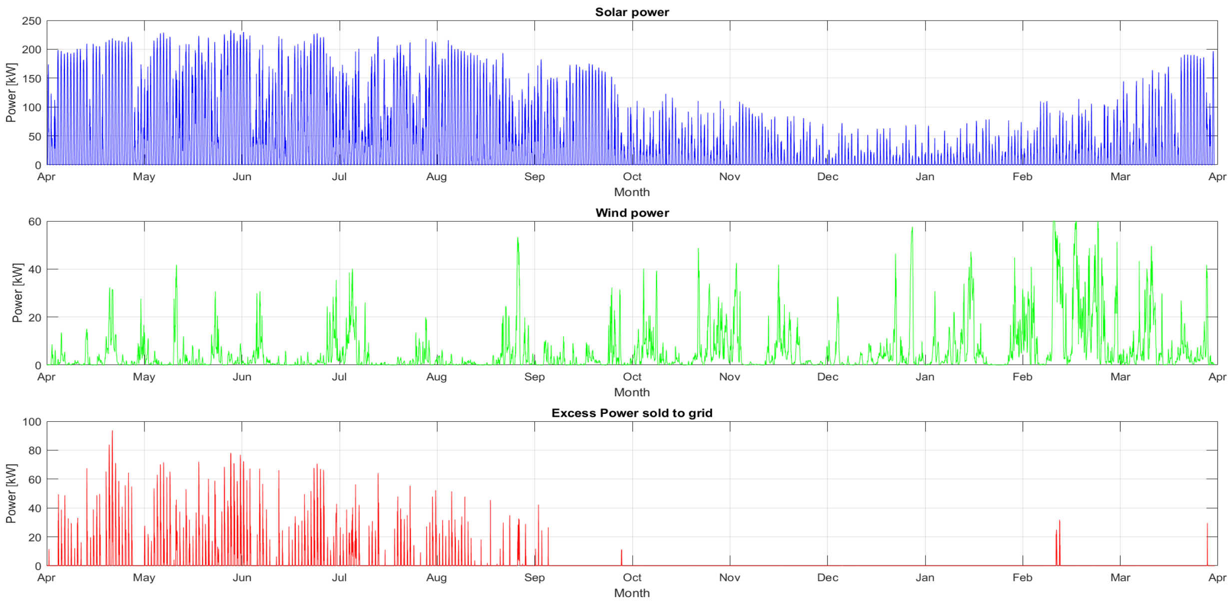

Figure 47: Total power production of solar panel, Excess electricity sold to the grid - scenario 3

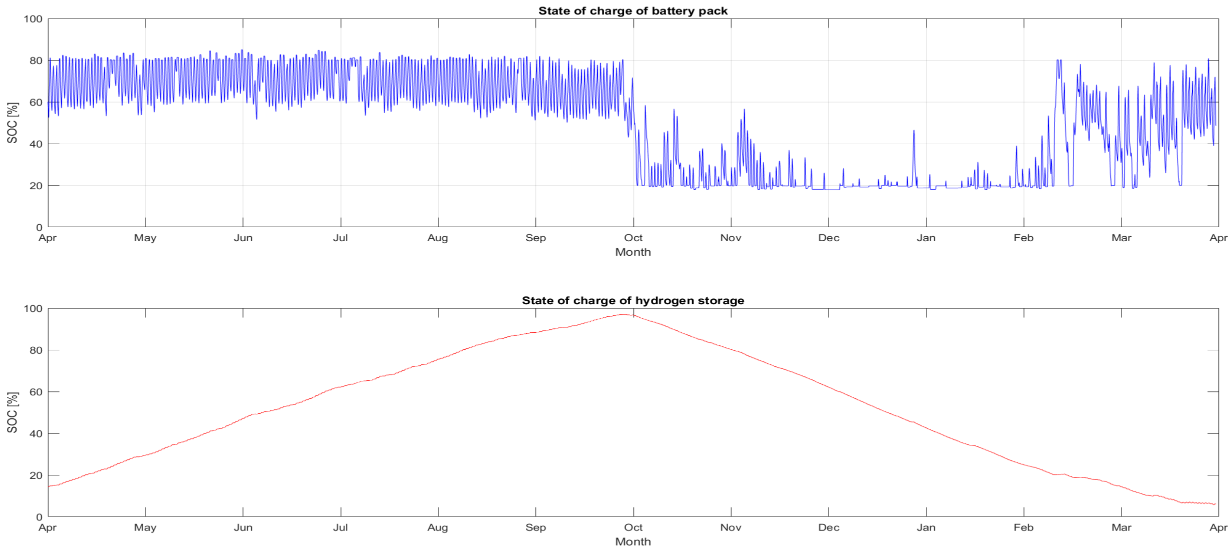

Figure 48: SOC of battery, SOC of hydrogen - scenario 3

Table 6: Overview of simulation results.

	Energy Demand (kWh)	Energy Production (kWh)	Energy sold to the grid (kWh)	% of production	Energy Loss (kWh)	Loss %
Scenario 1	170,877.5961	242,561.4031	17,972.9698	7.4097	53,801.5114	22.1806
Scenario 2	170,877.5961	245,286.0558	35,438.9818	14.498	38,969.4779	15.8879
Scenario 3	278,645.6586	361,216.1381	16,787.8097	4.6476	65,782.6699	18.2114

4.4.1 Economic Evaluation

Table 7: Comparison of three scenarios for sub components and their financial metrics

Scenario 1							
Component Name	**Capacity**	**Unit**	**CAPEX**	**OPEX/yr**	**Interest Rate**	**Lifetime (yr)**	**NPV (€)**
PV Panels	218	kW	52320	523	0.0270	15	58703.64
Wind Turbine	0	kW	0	0	0.027	15	0
Fuel Cell	45	kW	90000	3600	0.0270	15	133924.16
Electrolyser	100	kW	166600	4250	0.0270	15	218454.91
Battery	500	kWh	69500	2780	0.0270	15	103419.21
Hydrogen Storage	12000	ltr	240000	2400	0.0270	15	269282.71
Total			618420.00	13553.20			783784.70
Saving	170877.60	kWh	0	57244	0.0270	15	698442.87
Electricity to grid	17972.97	kWh		2696	0.0270	15	32893.65
Total NPV							-52448.18
Simple payback period			13.332 years	**Discounted payback period**			16.749 years
Scenario 2							
Component Name	**Capacity**	**Unit**	**CAPEX**	**OPEX/yr**	**Interest Rate**	**Lifetime (yr)**	**NPV (€)**
PV Panels	177	kW	42480	425	0.0270	15	47663.05
Wind Turbine	60	kW	105960	1060	0.0270	15	105960.00
Fuel Cell	45	kW	90000	3600	0.0270	15	133924.16
Electrolyser	100	kW	99960	2550	0.0270	15	131072.95
Battery	300	kWh	41700	1668	0.0270	15	62051.53
Hydrogen Storage	8000	ltr	160000	1600	0.0270	15	179521.85
Total			540100.00	10902.40			673121.88
Saving	170877.60	kWh	0	57244	0.0270	15	698442.87
Electricity to grid	35438.00	kWh		5316	0.0270	15	64857.68
Total NPV							90178.68
Simple payback period			10.455 years	**Discounted payback period**			12.450 years
Scenario 3							
Component Name	**Capacity**	**Unit**	**CAPEX**	**OPEX/yr**	**Interest Rate**	**Lifetime (yr)**	**NPV (€)**
PV Panels	280	kW	67200	672	0.0270	15	75399.18
Wind Turbine	60	kW	105960	1060	0.0270	15	118884.00
Fuel Cell	70	kW	140000	5600	0.0270	15	208326.47
Electrolyser	140	kW	233240	5950	0.0270	15	305387.36
Battery	700	kWh	97300	3892	0.0270	15	144786.90
Hydrogen Storage	26000	ltr	520000	5200	0.0270	15	583446.41
Total			1163700.00	22373.60			1436683.77
Saving	170877.60	kWh	0	57244	0.0270	15	755686.87
Saving - gas	46638.00	m^3	0	62029	0.027	15	756819.85
Electricity to grid	16787.80	kWh		2518	0.0270	15	30724.58
Total NPV							49303.54
Simple payback period			11.705 years	**Discounted payback period**			14.258 years

5 Conclusion and Recommendations

The project aimed to design an energy-independent system for the Rosandepolder community by integrating renewable energy sources with battery and hydrogen-based storage solutions. Through comprehensive analysis and simulation, the following conclusions are drawn:
The integration of solar photovoltaic (PV) panels and wind turbines was found to be the most effective combination of renewable energy sources. Solar PV panels, due to their high efficiency and availability, and wind turbines, providing additional energy during the winter months, together ensure a continuous and stable energy supply throughout the year.
To achieve energy independence, it was necessary to identify the optimal specifications for the energy storage components. The study concluded that a battery capacity of 300-700 kWh, utilizing lithium-ion technology, provides the necessary storage to manage daily energy fluctuations and maintain supply during periods of low renewable generation. In Scenario 1, with only PV panels, a battery capacity of 500 kWh was required. In Scenario 2, which included both PV panels and a wind turbine, the battery capacity was reduced to 300 kWh due to the additional energy contribution from the wind turbine. In Scenario 3, which also accounted for heating needs using heat pumps, the battery capacity needed was increased to 700 kWh to handle the higher energy demand.
Additionally, the hydrogen storage system, with an optimal electrolyser capacity of 100-140 kW and a storage capacity of 8,000-26,000 liters, ensures long-term energy storage. This system converts excess electricity into hydrogen during peak production times and generates electricity through a fuel cell, sized between 45-70 kW, when renewable generation is insufficient. Specifically, in Scenario 1, the electrolyser capacity was 100 kW, hydrogen storage was 12,000 liters, and the fuel cell capacity was 45 kW. In Scenario 2, the electrolyser capacity was reduced to 60 kW, hydrogen storage to 8,000 liters, and the fuel cell capacity remained at 45 kW. In Scenario 3, the electrolyser capacity increased to 140 kW, hydrogen storage to 26,000 liters, and the fuel cell capacity to 70 kW to meet the higher energy demand including heating.
The economic feasibility of the proposed system was assessed through net present value (NPV) and payback period calculations. The scenarios analyzed revealed varying degrees of economic viability. Scenario 2 presented the best economic outcome with a positive NPV of €90,178.68 and a discounted payback period of 12.45 years, indicating economic sustainability. Scenario 1 had a negative NPV of €-52,448.18 with a discounted payback period of 16.75 years, while Scenario 3 balanced energy supply and demand effectively, presenting a viable long-term solution despite a longer payback period.
Overall, the project successfully demonstrated that an energy-independent system for the Rosandepolder community is achievable through the strategic integration of solar PV, wind energy, and hybrid storage solutions. The proposed system meets the community's energy demands, aligns with sustainability goals, reduces reliance on fossil fuels, and contributes to the reduction of greenhouse gas emissions.
Based on the findings and conclusions of this project, the following recommendations are made for future research:

- Validate the complete model with the real life actual system.
- Investigate the potential for integrating additional renewable energy sources, such as biomass or geothermal energy, to diversify the energy mix and enhance reliability.
- Conduct detailed site-specific studies to optimize the placement and orientation of PV panels and wind turbines to maximize energy capture and efficiency.
- Explore the use of advanced battery technologies, and other energy storage methods.

References

Abo-Khalil, A. G., Alyami, S., Sayed, K., & Alhejji, A. (2019, May). Dynamic modeling of wind turbines based on estimated wind speed under turbulent conditions. *Energies*, *12*(10), 1907. Retrieved from http://dx.doi.org/10.3390/en12101907 doi: 10.3390/en12101907

Alonso, A. M., Costa, D., Messagie, M., & Coosemans, T. (2024). Techno-economic assessment on hybrid energy storage systems comprising hydrogen and batteries: A case study in belgium. *International Journal of Hydrogen Energy*, *52*, 1124–1135.

Azari, D. (2020). *Future urban energy systems: Harnessing demand side flexibility and managing data uncertainty* (Unpublished doctoral dissertation). Wageningen University and Research.

Badami, A., Mcgrath, J., Davis, R., Joseph, E., Riffle, J., & Wilkes, G. (n.d.). Morphological and structure-property analyses of poly(arylene ether sulfone)-based random and multiblock copolymers for fuel cells.

Carriveau, R. (2011). *Fundamental and advanced topics in wind power*. BoD–Books on Demand.

Cheng, Q., Zhang, R., Shi, Z., & Lin, J. (2024). Review of common hydrogen storage tanks and current manufacturing methods for aluminium alloy tank liners. *International Journal of Lightweight Materials and Manufacture*, *7*(2), 269-284. Retrieved from https://www.sciencedirect.com/science/article/pii/S2588840423000434 doi: https://doi.org/10.1016/j.ijlmm.2023.08.002

Christ, F., & Abeykoon, C. (2015, September). Modelling of a wind power turbine. In *2015 internet technologies and applications (ita).* IEEE. Retrieved from http://dx.doi.org/10.1109/ITechA.2015.7317396 doi: 10.1109/itecha.2015.7317396

Correa, J., Farret, F., Popov, V., & Simoes, M. (2005). Sensitivity analysis of the modeling parameters used in simulation of proton exchange membrane fuel cells. *IEEE Transactions on Energy Conversion*, *20*(1), 211-218. doi: 10.1109/TEC.2004.842382

Cylinders, L. G. (2024, 3). *Home - Luxfer Gas cylinders.* Retrieved from https://www.luxfercylinders.com/ (Accessed: Apr 29, 2024)

Database - Eurostat. (n.d.). Retrieved from https://ec.europa.eu/eurostat/web/energy/database (Accessed: Mar 17, 2024)

De Silva, Y., & Middleton, P. (2017). *Design of an alkaline electrolysis stack* (Doctoral dissertation). doi: 10.13140/RG.2.2.14351.12964

Dimpl, E. (2010). Small-scale electricity generation from biomass. *Part I: biomass gasification, 1st edn. GTZ-HERA. Poverty-oriented Basic Energy Service*.

Dwivedi, P., Sudhakar, K., Soni, A., Solomin, E., & Kirpichnikova, I. (2020). Advanced cooling techniques of p.v. modules: A state of art. *Case Studies in Thermal Engineering*, *21*, 100674. Retrieved from https://www.sciencedirect.com/science/article/pii/S2214157X19305416 doi: 10.1016/j.csite.2020.100674

Díaz-González, F., Sumper, A., Bellmunt, O., & Villafafila-Robles, R. (2012, 05). A review of energy storage technologies for wind power applications. *Renewable and Sustainable Energy Reviews*, *16*, 2154-2171. doi: 10.1016/j.rser.2012.01.029

Díaz-González, F., Sumper, A., Gomis-Bellmunt, O., & Villafáfila-Robles, R. (2012). A review of energy storage technologies for wind power applications. *Renewable and Sustainable Energy Reviews*, *16*(4), 2154-2171. Retrieved from https://www.sciencedirect.com/science/article/pii/S1364032112000305 doi: https://doi.org/10.1016/j.rser.2012.01.029

EcoProgetti. (2021, 7). *The structure of a photovoltaic module.* Retrieved from https://ecoprogetti.com/the-structure-of-photovoltaic-module/ (Accessed: Mar 17, 2024)

Edited in canva.com. (n.d.). Retrieved from https://www.canva.com/ (Accessed: Apr 19, 2024)

El Hammoumi, A., Chtita, S., Motahhir, S., & El Ghzizal, A. (2022). Solar pv energy: From material to use, and the most commonly used techniques to maximize the power output of pv systems: A focus on solar trackers and floating solar panels. *Energy Reports*, *8*, 11992-12010. Retrieved from https://www.sciencedirect.com/science/article/pii/S2352484722017784 doi: https://doi.org/10.1016/j.egyr.2022.09.054

Electrolyser cost—EHO. (n.d.). Retrieved from https://observatory.clean-hydrogen.europa.eu/hydrogen-landscape/production-trade-and-cost/electrolyser-cost

El-Shafie, M., Kambara, S., & Hayakawa, Y. (2019). Hydrogen production technologies overview. *Journal of Power and Energy Engineering*, *07*(01), 107–154. Retrieved from http://dx.doi.org/10.4236/jpee.2019.71007 doi: 10.4236/jpee.2019.71007

Energy.gov. (n.d.). *Clean energy sources.* Retrieved from https://www.energy.gov/clean-energy (Accessed: Feb 04, 2024)

Fernando, J. (2024, 3). *Net Present Value (NPV): what it means and steps to calculate it.* Retrieved from https://www.investopedia.com/terms/n/npv.asp (Accessed: Apr 29, 2024)

FLEXPOWER. (2023, 12). *What is a Battery Energy Storage System (BESS)? — Definition.* Retrieved from https://flex-power.energy/school-of-flex/battery-energy-storage-system-bess/

for Climate, C., & Solutions, E. (2019, 12). OUTCOMES OF THE U.N. CLIMATE CHANGE CONFERENCE IN MADRID. *INTERNATIONAL.* Retrieved from https://www.c2es.org/wp-content/uploads/2019/12/cop-25-madrid-summary-1.pdf

Garcia-Torres, F. (2015). *Advanced control of renewable energy microgrids with hybrid energy storage system* (Doctoral dissertation). doi: 10.13140/RG.2.1.4380.7762

Hassan, Q., Jaszczur, M., & Przenzak, E. (2017). Mathematical model for the power generation from arbitrarily oriented photovoltaic panel. *E3S Web of Conferences*, *14*, 01028. Retrieved from http://dx.doi.org/10.1051/e3sconf/20171401028 doi: 10.1051/e3sconf/20171401028

Hyder, Z. (n.d.). *Solar system types compared: Grid-Tied, Off-Grid, and Hybrid.* Retrieved from https://www.solarreviews.com/blog/grid-tied-off-grid-and-hybrid-solar-systems (Accessed: Apr 29, 2024)

Iea. (n.d.). *Electrolysers - energy system.* Retrieved from https://www.iea.org/energy-system/low-emission-fuels/electrolysers (Accessed: Apr 19, 2024)

Jacobson, M. Z. (2009). Review of solutions to global warming, air pollution, and energy security. *Energy Environ. Sci.*, *2*, 148-173. Retrieved from http://dx.doi.org/10.1039/B809990C doi: 10.1039/B809990C

Johnson, S. C., Rhodes, J. D., & Webber, M. E. (2020). Understanding the impact of non-synchronous wind and solar generation on grid stability and identifying mitigation pathways. *Applied Energy*, *262*, 114492. Retrieved from https://www.sciencedirect.com/science/article/pii/S0306261920300040 doi: https://doi.org/10.1016/j.apenergy.2020.114492

KIJO Battery. (n.d.). Retrieved from https://www.kijo-battery.com/off-grid-energy-storage-system.html (Accessed: Apr 29, 2024)

Lane, C. (n.d.). *Types of solar panels: which one is the best choice?* Retrieved from https://www.solarreviews.com/blog/pros-and-cons-of-monocrystalline-vs-polycrystalline-solar-panels#:~:text=Polycrystalline\%20solar\%20panels\%20are\%20cheaper,to\%20meet\%20your\%20energy\%20needs. (Accessed: Mar 17, 2024)

Li, B. (2018a). *Sizing and Operation of Multi-Energy Hydrogen-Based Microgrids* (Theses, Université Bourgogne Franche-Comté). Retrieved from https://theses.hal.science/tel-02077668

Li, B. (2018b). *Sizing and Operation of Multi-Energy Hydrogen-Based Microgrids* (Theses, Université Bourgogne Franche-Comté). Retrieved from https://theses.hal.science/tel-02077668

Li, J., Li, G., Ma, S., Liang, Z., Li, Y., & Zeng, W. (2023a). Modeling and simulation of hydrogen energy storage system for power-to-gas and gas-to-power systems. *Journal of Modern Power Systems and Clean Energy*, *11*(3), 885–895. Retrieved from http://dx.doi.org/10.35833/MPCE.2021.000705 doi: 10.35833/mpce.2021.000705

Li, J., Li, G., Ma, S., Liang, Z., Li, Y., & Zeng, W. (2023b). Modeling and simulation of hydrogen energy storage system for power-to-gas and gas-to-power systems. *Journal of Modern Power Systems and Clean Energy*, *11*(3), 885-895. doi: 10.35833/MPCE.2021.000705

Mann, R. F., Amphlett, J. C., Hooper, M. A., Jensen, H. M., Peppley, B. A., & Roberge, P. R. (2000). Development and application of a generalised steady-state electrochemical model for a pem fuel cell. *Journal of Power Sources*, *86*(1), 173-180. Retrieved from https://www.sciencedirect.com/science/article/pii/S037877539900484X doi: https://doi.org/10.1016/S0378-7753(99)00484-X

Manyonge, A., Manyala, R., Onyango, F., & Shichika, J. (2012, 01). Mathematical modelling of wind turbine in a wind energy conversion system: Power coefficient analysis. *Applied Mathematical Sciences*, *6*, 4527-4536.

McKendry, P. (2002). Energy production from biomass (part 1): overview of biomass. *Bioresource Technology*, *83*(1), 37-46. Retrieved from https://www.sciencedirect.com/science/article/pii/S0960852401001183 (Reviews Issue) doi: https://doi.org/10.1016/S0960-8524(01)00118-3

Melaina, M. W., Antonia, O., & Penev, M. (2013). Blending hydrogen into natural gas pipeline networks: a review of key issues.

Mertens, S. (2022). Design of wind and solar energy supply, to match energy demand. *Cleaner Engineering and Technology*, *6*, 100402. Retrieved from https://www.sciencedirect.com/science/article/pii/S2666790822000076 doi: https://doi.org/10.1016/j.clet.2022.100402

Metabolic. (2020, 2). *Smart Integrated Decentralised Energy (SIDE) Systems.* Retrieved from https://www.metabolic.nl/publication/new-strategies-for-smart-integrated-decentralised-energy-systems/\#The_energy_transition (Accessed: Apr 29, 2024)

Miller, E. L., Peterson, D., Randolph, K., & Ainscough, C. (2014). Critical metrics and fundamental materials challenges for renewable hydrogen production technologies. *MRS Online Proceedings Library (OPL)*, *1669*, mrss14–1669.

mitsubushi heavy indrustries group. (n.d.). Retrieved from https://solutions.mhi.com/clean-fuels/h2-compressor/ (Accessed: Mar 17, 2024)

Munguia, S. F. (2023, 9). *Wind turbines for very low winds, the future of wind energy?* Retrieved from https://www.linkedin.com/pulse/wind-turbines-very-low-winds-future-energy-sergio-fernandez-munguia/

Netherlands, S. (2024, 3). Nearly half the electricity produced in the Netherlands is now renewable. Retrieved from https://www.cbs.nl/en-gb/news/2024/10/nearly-half-the-electricity-produced-in-the-netherlands-is-now-renewable#:~:text=Nearly\%20half\%20the\%20electricity\%20produced\%20in\%20the\%20Netherlands\%20is\%20now\%20renewable,-07\%2F03\%2F2024\&text=A\%20total\%20of\%20120\%20billion,percent\%20from\%20the\%20previous\%20year.

Netherlands-Statistics(CBS). (2023, 6). Renewable energy share rose to 15 percent in 2022. Retrieved from https://www.cbs.nl/en-gb/news/2023/22/renewable-energy-share-rose-to-15-percent-in-2022

Nguyen, X. H., & Nguyen, M. P. (2015, December). Mathematical modeling of photovoltaic cell/module/arrays with tags in matlab/simulink. *Environmental Systems Research*, *4*(1).

Retrieved from http://dx.doi.org/10.1186/s40068-015-0047-9 doi: 10.1186/s40068-015-0047-9

Noro, Y., & Uchiyama, S. (2021, October). Use of hydrogen storage in an off-grid system for implementing a renewable-energy system. *Clean Energy*, *5*(4), 704–712. Retrieved from http://dx.doi.org/10.1093/ce/zkab043 doi: 10.1093/ce/zkab043

Nortier, N., Paardekooper, M., Lucas, C., Blankert, A., van der Neut, A., Luxembourg, S., ... van Sark, W. (2023, July). Spatially resolved generation profiles for building, land and water-bound pv: a case study of four dutch energy transition scenarios. *Advances in Geosciences*, *58*, 199–216. Retrieved from http://dx.doi.org/10.5194/adgeo-58-199-2023 doi: 10.5194/adgeo-58-199-2023

Parthiban, R., & Ponnambalam, P. (2022). An enhancement of the solar panel efficiency: A comprehensive review. *Frontiers in Energy Research*, *10*. Retrieved from https://www.frontiersin.org/articles/10.3389/fenrg.2022.937155 doi: 10.3389/fenrg.2022.937155

pvgis.com. (n.d.). Retrieved from https://pvgis.com/ (Accessed: Apr 29, 2024)

Q CELLS G5 320W Solar Panel. (n.d.). Retrieved from https://www.solarelectricsupply.com/solar-panels/q-cells/q-cells-q-peak-duo-g5-320-watt-solar-panel (Accessed: Apr 29, 2024)

Ramos Hernanz, J., Campayo Martín, J., Zamora Belver, I., Larrañaga Lesaka, J., Zulueta Guerrero, E., & Puelles Pérez, E. (2010, April). Modelling of photovoltaic module. *Renewable Energy and Power Quality Journal*, *1*(08), 1186–1190. Retrieved from http://dx.doi.org/10.24084/repqj08.619 doi: 10.24084/repqj08.619

Roman, K., Barwicki, J., Hryniewicz, M., Szadkowska, D., & Szadkowski, J. (2021). Production of electricity and heat from biomass wastes using a converted aircraft turbine ai-20. *Processes*, *9*(2). Retrieved from https://www.mdpi.com/2227-9717/9/2/364 doi: 10.3390/pr9020364

Rosandepolder. (2023, May). Retrieved from https://rosandepolderoosterbeek.nl/geschiedenis/ (Accessed: Mar 17, 2024)

Serra, F., Lucariello, M., Petrollese, M., & Cau, G. (2020). Optimal integration of hydrogen-based energy storage systems in photovoltaic microgrids: A techno-economic assessment. *Energies*, *13*(16). Retrieved from https://www.mdpi.com/1996-1073/13/16/4149 doi: 10.3390/en13164149

Spector, J., & McCarthy, D. (2023, 12). Chart: Lithium-ion battery prices are falling again. Retrieved from https://www.canarymedia.com/articles/batteries/chart-lithium-ion-battery-prices-are-falling-again

SRO, V. A. (n.d.). *8 Types of fuel cell by price point.* Retrieved from https://www.horizoneducational.com/8-types-of-fuel-cell-by-price-point/t1418?currency=usd\#:~:text=The\%20fuel\%20cell\%20price\%20can,be\%20as\%20high\%20as\%20\%24\%2015\%2C000.

Sun, Z., Kong, L., Wang, X., Lei, Y., Li, X., Tang, H., ... Chang, Z. (2023, March). Study of the electrochemical properties of fe3o4/c–bi composites prepared by spray drying and their use in cylindrical sealed nickel iron batteries. *International Journal of Hydrogen Energy*, *48*(26), 9785–9796. Retrieved from http://dx.doi.org/10.1016/j.ijhydene.2022.11.241 doi: 10.1016/j.ijhydene.2022.11.241

Teyabeen, A., Akkari, F., & Jwaid, A. (2019, January). Mathematical modelling of wind turbine power curve. *International journal of simulation: systems, science & technology*. Retrieved from http://dx.doi.org/10.5013/IJSSST.a.19.05.15 doi: 10.5013/ijssst.a.19.05.15

Thapar, V., Agnihotri, G., & Sethi, V. K. (2011). Critical analysis of methods for mathematical modelling of wind turbines. *Renewable Energy*, *36*(11), 3166-3177. Retrieved from https://www.sciencedirect.com/science/article/pii/S0960148111001303 doi:

https://doi.org/10.1016/j.renene.2011.03.016

Thoubboron, K. (2018, 8). *60 Cell vs. 72 Cell Solar Panels: Which is Right For You?* Retrieved from https://www.energysage.com/solar/solar-photovoltaic-cells/60-vs-72-cell-solar-panels-which-is-right/ (Accessed: Mar 17, 2024)

Tian, H., Mancilla-David, F., Ellis, K., Muljadi, E., & Jenkins, P. (2012, 07). Detailed performance model for photovoltaic systems: Preprint.

Turton, R., Bailie, R. C., Whiting, W. B., & Shaeiwitz, J. A. (2008). *Analysis, synthesis and design of chemical processes.* Pearson Education.

University, B. (2020, Mar). *What's the best battery?* Retrieved from https://batteryuniversity.com/article/whats-the-best-battery (Accessed: Mar 17, 2024)

Ural Bayrak, Z., & Gençoğlu, M. (2010, 01). Mathematical models of pem fuel cells. *Proc. 5th Int. Ege Energy Symp. Exhib.*

van Economische Zaken en Klimaat, M. (2019, September). *Climate agreement.* Report. Retrieved from https://www.government.nl/documents/reports/2019/06/28/climate-agreement (Accessed: Feb 04, 2024)

YİĞİT, C. (2017). Wind turbine blade design with computational fluid dynamics analysis. *International Journal of Computational and Experimental Science and Engineering*, *3*(2), 44–49.

Zhu, L., Yu, Q., Huang, Y., Guan, J., Wang, Y., & Yan, Y. (2020, March). Mathematical modelling and operation parameters analysis of proton exchange membrane fuel cell. *IOP Conference Series: Earth and Environmental Science*, *467*(1), 012071. Retrieved from http://dx.doi.org/10.1088/1755-1315/467/1/012071 doi: 10.1088/1755-1315/467/1/012071

Øystein Ulleberg. (2003). Modeling of advanced alkaline electrolyzers: a system simulation approach. *International Journal of Hydrogen Energy*, *28*(1), 21-33. Retrieved from https://www.sciencedirect.com/science/article/pii/S0360319902000332 doi: https://doi.org/10.1016/S0360-3199(02)00033-2

APPENDIX A: Parameters for Model

Table 8: Parameters description, nomenclature, unit, values its Sources

Parameter Description	Symbol	Unit	Value	Source
Photovoltaic panel				
Rated Power at STC	P_{max}	W	320	Data-sheet(*Q CELLS G5 320W Solar Panel*, n.d.)
Open circuit voltage	V_{oc}	V	45.48	Data-sheet(*Q CELLS G5 320W Solar Panel*, n.d.)
Short circuit current	I_{sc}	A	8.60	Data-sheet(*Q CELLS G5 320W Solar Panel*, n.d.)
PV module efficiency	η_{pv}	$-$	18.20	Data-sheet(*Q CELLS G5 320W Solar Panel*, n.d.)
No of solar cells in 1 module	N_c	$-$	72	(*Q CELLS G5 320W Solar Panel*, n.d.)
Charge of en electron	q	C	1.602×10^{-19}	(Ramos Hernanz et al., 2010)
Boltzmann constant	k	J/K	1.38065×10^{-23}	-
Ideality factor	n	-	1.3	(Garcia-Torres, 2015)
Equivalent series resistance	R_s	Ω	0.223	(Garcia-Torres, 2015)
Equivalent shunt resistance	R_{sh}	Ω	415	(Garcia-Torres, 2015)
Short circuit current temperature coefficient	K_i	A/K	0.0005	Data-sheet(*Q CELLS G5 320W Solar Panel*, n.d.)
Band gap energy of semiconductor	E_g	eV	1.1	(Nguyen & Nguyen, 2015)
Normal operating cell temperature	NOCT	$^{\circ}C$	45	(*Q CELLS G5 320W Solar Panel*, n.d.)
No. of panels	N_{PV}		simulation	
Irradiation at standard test condition	G_{STC}	W/m^2	1000	(*Q CELLS G5 320W Solar Panel*, n.d.)
Cell temperature at STC	T_{STC} of cell	$^{\circ}C$	25	Data-sheet(*Q CELLS G5 320W Solar Panel*, n.d.)
Irradiation at NOCT	G_{NOCT}	W/m^2	800	(*Q CELLS G5 320W Solar Panel*, n.d.)
Temperature coefficient for power	α_p	%	-0.04	(*Q CELLS G5 320W Solar Panel*, n.d.)
Electrolyser				
Electrolyser surface area	A	m^2	0.25	Assumed
Faraday's constant	F	C/mol	96485	(Øystein Ulleberg, 2003)
Parameter related to ohmic resistance of Alkaline electrolyser	r_1	Ωm^2	8.05×10^{-5}	(Øystein Ulleberg, 2003)
	r_2	$\Omega m^2/^{\circ}C$	$-2.5 \times 10^{-}$	(Øystein Ulleberg, 2003)
Coefficient for overvoltage on electrodes	s	V	0.185	(Øystein Ulleberg, 2003)
	t_1	m^2/A	-1.002	(Øystein Ulleberg, 2003)
	t_2	$m^{2\circ}C/A$	8.424	(Øystein Ulleberg, 2003)
	t_3	m^2K^2/A	247.3	(Øystein Ulleberg, 2003)
Faraday efficiency parameter	f_1	mA^2cm^4	250	(Øystein Ulleberg, 2003)
	f_2	$-$	0.98	(Øystein Ulleberg, 2003)

Parameters	Symbol	Unit	Value	Source
Hydrogen storage system				
Efficiency of compressor	η_{comp}	%	85	Assumed
Specific heat capacity of hydrogen at constant pressure	C_{pH_2}	kJ/kg.K	14.05	(J. Li et al., 2023b)
Specific heat ratio of hydrogen under standard condition	k	-	1.414	(J. Li et al., 2023b)
Molar gas constant	R	$J/mol.K$	8.3145	
Volume of storage tank	V_{tank}	$-$	0.905	Calculated by simulation
Temperature of gas inside storage	T_{tank}	$^{\circ}C$	50	Assumed
PEM Fuel cell				
Operating temperature of fuel cell	T	K	333.15	Assumed
Partial pressure of oxygen in air	P_{O_2}	atm	0.21	(Correa et al., 2005)
Partial pressure of hydrogen	P_{H_2}	atm	1	(Correa et al., 2005)
Parametric coefficients	ζ_1	-	-0.948	(Correa et al., 2005)
	ζ_2	-	$0.00286 + 0.0002\ln(A) + 4.3\times10^{-5}\ln(C_{H_2})$	(Correa et al., 2005)
	ζ_3	-	7.6×10^{-5}	(Correa et al., 2005)
	ζ_4	-	-1.93×10^{-4}	(Correa et al., 2005)
Thickness of Nafion 117 membrane	l	μm	178	(Correa et al., 2005),(Mann et al., 2000)
Area of membrane	A	cm^2	64	(Correa et al., 2005)
Specific coefficient of membrane	ψ	-	23	(Correa et al., 2005)
Constant for concentration overvoltage	B	V	0.016	(Correa et al., 2005)
Maximum current density of membrane	J_{max}	mA/cm^2	469	(Correa et al., 2005)
Permanent current density	J_{min}	mA/cm^2	3	(Correa et al., 2005)
Equivalent contact resistance	R_C	Ω	0.0003	(Correa et al., 2005)
Battery storage				
Nominal capacity of battery	C_{nom}	kWh	simulation	
Charging efficiency	η_{ch}	%	98	assumed
Discharging efficiency	η_{dis}	%	97	assumed
Economic calculations				
Interest rate	i	%	2.7	
Life period	n	years	15	

APPENDIX B: Data Sheet of PV panel

Q.PEAK DUO BLK-G5 305-320

Q.ANTUM SOLAR MODULE

The new Q.PEAK DUO BLK-G5 solar module from Q CELLS impresses with its outstanding visual appearance and particularly high performance on a small surface thanks to the innovative Q.ANTUM DUO Technology. Q.ANTUM's world-record-holding cell concept has now been combined with state-of-the-art circuitry half cells and a six-busbar design, thus achieving outstanding performance under real conditions — both with low-intensity solar radiation as well as on hot, clear summer days.

Q.ANTUM TECHNOLOGY: LOW LEVELISED COST OF ELECTRICITY
Higher yield per surface area, lower BOS costs, higher power classes, and an efficiency rate of up to 19.3 %.

INNOVATIVE ALL-WEATHER TECHNOLOGY
Optimal yields, whatever the weather with excellent low-light and temperature behaviour.

ENDURING HIGH PERFORMANCE
Long-term yield security with Anti LID Technology, Anti PID Technology[1], Hot-Spot Protect and Traceable Quality Tra.Q™.

EXTREME WEATHER RATING
High-tech aluminium alloy frame, certified for high snow (5400 Pa) and wind loads (4000 Pa).

A RELIABLE INVESTMENT
Inclusive 12-year product warranty and 25-year linear performance warranty[2].

STATE OF THE ART MODULE TECHNOLOGY
Q.ANTUM DUO combines cutting edge cell separation and innovative wiring with Q.ANTUM Technology.

EUPD RESEARCH TOP BRAND PV MODULES EUROPE 2017

Q CELLS YIELD SECURITY: ANTI PID TECHNOLOGY (APT), HOT-SPOT PROTECT (HSP), TRACEABLE QUALITY (TRA.Q™), ANTI LID TECHNOLOGY (ALT)

VDE Quality Tested 11/2016 – high reliability, low degradation, optimized durability, continous line monitoring – www.VDEinfo.com ID. 40032587

pv magazine award 2017 top innovation

[1] APT test conditions according to IEC/TS 62804-1:2015, method B (−1500 V, 168 h)
[2] See data sheet on rear for further information.

THE IDEAL SOLUTION FOR:

Rooftop arrays on residential buildings

Engineered in **Germany**

Q CELLS

MECHANICAL SPECIFICATION

Format	1685 mm × 1000 mm × 32 mm (including frame)
Weight	18.7 kg
Front Cover	3.2 mm thermally pre-stressed glass with anti-reflection technology
Back Cover	Composite film
Frame	Black anodised aluminium
Cell	6 × 20 monocrystalline Q.ANTUM solar half cells
Junction box	70-85 mm × 50-70 mm × 13-21 mm Protection class IP67, with bypass diodes
Cable	4 mm² Solar cable; (+) 1100 mm, (–) 1100 mm
Connector	Multi-Contact MC4, IP65 and IP68

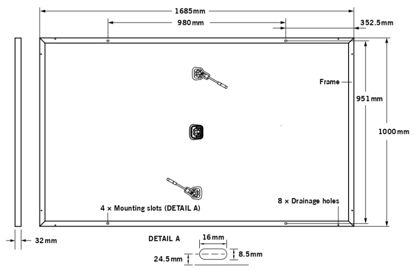

ELECTRICAL CHARACTERISTICS

POWER CLASS				305	310	315	320
MINIMUM PERFORMANCE AT STANDARD TEST CONDITIONS, STC[1] (POWER TOLERANCE +5 W / −0 W)							
Minimum	Power at MPP[2]	P_{MPP}	[W]	305	310	315	320
Minimum	Short Circuit Current*	I_{SC}	[A]	9.78	9.83	9.89	9.94
Minimum	Open Circuit Voltage*	V_{OC}	[V]	39.75	40.02	40.29	40.56
Minimum	Current at MPP*	I_{MPP}	[A]	9.31	9.36	9.41	9.47
Minimum	Voltage at MPP*	V_{MPP}	[V]	32.78	33.12	33.46	33.80
Minimum	Efficiency[2]	η	[%]	≥ 18.1	≥ 18.4	≥ 18.7	≥ 19.0
MINIMUM PERFORMANCE AT NORMAL OPERATING CONDITIONS, NOC[3]							
Minimum	Power at MPP[2]	P_{MPP}	[W]	226.0	229.7	233.5	237.2
Minimum	Short Circuit Current*	I_{SC}	[A]	7.88	7.93	7.97	8.02
Minimum	Open Circuit Voltage*	V_{OC}	[V]	37.18	37.43	37.69	37.94
Minimum	Current at MPP*	I_{MPP}	[A]	7.32	7.36	7.41	7.45
Minimum	Voltage at MPP*	V_{MPP}	[V]	30.88	31.20	31.52	31.84

[1] 1000 W/m², 25 °C, spectrum AM 1.5 G [2] Measurement tolerances STC ± 3 %; NOC ± 5 % [3] 800 W/m², NOCT, spectrum AM 1.5 G * typical values, actual values may differ

Q CELLS PERFORMANCE WARRANTY

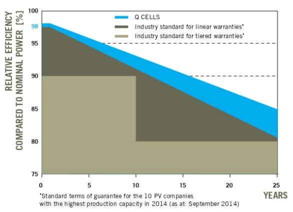

At least 98 % of nominal power during first year. Thereafter max. 0.54 % degradation per year. At least 93.1 % of nominal power up to 10 years. At least 85 % of nominal power up to 25 years.

All data within measurement tolerances. Full warranties in accordance with the warranty terms of the Q CELLS sales organisation of your respective country.

PERFORMANCE AT LOW IRRADIANCE

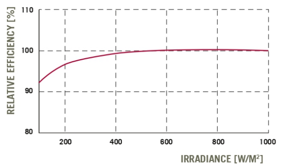

Typical module performance under low irradiance conditions in comparison to STC conditions (25 °C, 1000 W/m²).

TEMPERATURE COEFFICIENTS

Temperature Coefficient of I_{SC}	α	[% / K]	+0.04	**Temperature Coefficient of V_{OC}**	β	[% / K]	−0.28
Temperature Coefficient of P_{MPP}	γ	[% / K]	−0.37	**Normal Operating Cell Temperature**	NOCT	[°C]	45

PROPERTIES FOR SYSTEM DESIGN

Maximum System Voltage	V_{SYS}	[V]	1000	**Safety Class**	II
Maximum Reverse Current	I_R	[A]	20	**Fire Rating**	C
Push / Pull Load (Test-load in accordance with IEC 61215)		[Pa]	5400 / 4000	**Permitted Module Temperature On Continuous Duty**	-40 °C up to +85 °C

QUALIFICATIONS AND CERTIFICATES

VDE Quality Tested, IEC 61215 (Ed. 2); IEC 61730 (Ed. 1), Application class A
This data sheet complies with DIN EN 50380.

PARTNER

NOTE: Installation instructions must be followed. See the installation and operating manual or contact our technical service department for further information on approved installation and use of this product.

Hanwha Q CELLS GmbH
Sonnenallee 17-21, 06766 Bitterfeld-Wolfen, Germany | **TEL** +49 (0)3494 66 99-23444 | **FAX** +49 (0)3494 66 99-23000 | **EMAIL** sales@q-cells.com | **WEB** www.q-cells.com

Engineered in **Germany**

APPENDIX C: Data Sheet of Wind Turbine

Ryse Energy www.ryse.energy

E-60
DATA SHEET

GENERATOR	Type	Permanent Magnet
	Maximum Power	70 kW
	Rated Power	60 kW
ROTOR	Configuration	Horizontal Axis
	No. of Blades	3
	Blade Material	Glass fibre
	Blade Length	7.4 m
	Rotor Diameter	15.8 m
	Swept Area	193 m^2
	Nominal Rotor Speed	120 rpm
	Pitch/Yaw	Downwind passive pitch
WIND	Cut-In Speed	2 m/s
	Rated Wind Speed	11 m/s
	Cut-Out Speed	30 m/s
	Survival Speed	59.5 m/s
WEIGHTS	Nacelle/Rotor	4,500 kg
TOWERS	Lattice	18 – 36 m
	Monopole	18 – 27 m
	Tilt-Up	18 – 27 m
DESIGN PARAMETERS	Turbine Design Class	IEC 61400-2 Class II
	Temperature Range	-20° to 50°C
	Lifespan & Servicing	20 years, subject to regular maintenance

TECHNICAL PROFILE

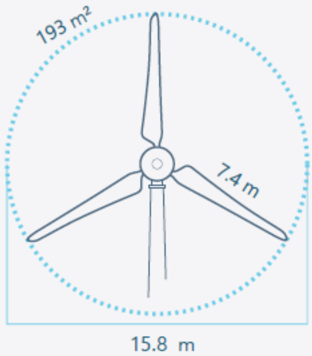

CLASS II

PASSIVE REGULATION

SAFETY

- Base Level: Active blade pitch control, with 90° of movement, limits power output and can put blades in a total stall position.
- Second Level: Electronic control system activates mechanical brake with shaft lock and electromagnetic induction brake.
- Third Level: Passive springs deploy, putting the turbine blades in a stall position, spoiling the rotor aerodynamics and subsequently its ability to rotate.

DATA INPUT & MANAGEMENT

- Remote Control: Allows the remote customization of the wind turbine in order for Ryse to provide optimum performance in every site.
- Storm Detection: Intelligent storm detection algorithm and automatic safety lock protect the turbine in the event of dangerous gusts/hurricane weather.
- LCD display in control box. Can output to local PC or be monitored remotely via the internet.

CONSTRUCTION & MAINTENANCE

- Anti-Corrosive Blades: The blades and nacelle are treated with epoxy paint and hermetically sealed. This gives corrosion and saline protection, making the turbine ideal for island, coastal or desert deployments.
- Ryse service contract available.

POWER CURVE*

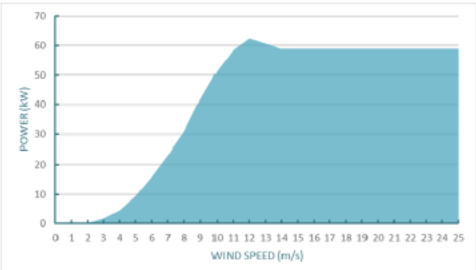

ENERGY OUTPUT*

Annual Mean Wind Speed (m/s)	Estimated Annual Output (kWh)
5.0	119,121
5.5	145,580
6.0	171,886
6.5	202,278
7.0	221,466
7.5	243,979
8.0	264,856

** Indicative power curve and estimated energy output. Based on ongoing testing.*

APPENDIX D: Input parameters (Solar irradiation(I), Ambient temperature (T_{amb}), Wind speed (V_{wind}) for simulation scenarios

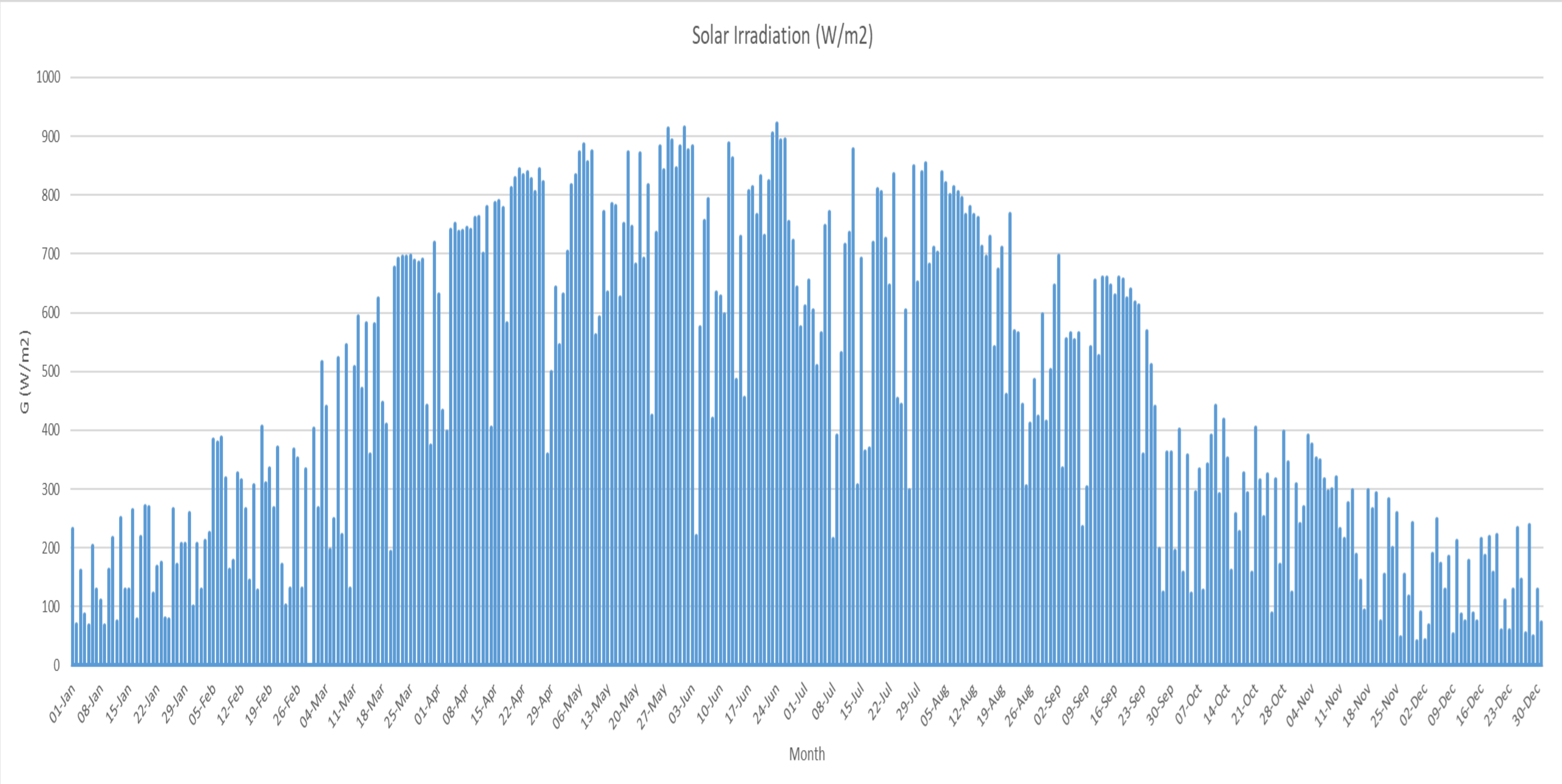

Figure 49: Daily irradiation data for whole year at Rosandepolder (*pvgis.com*, n.d.)

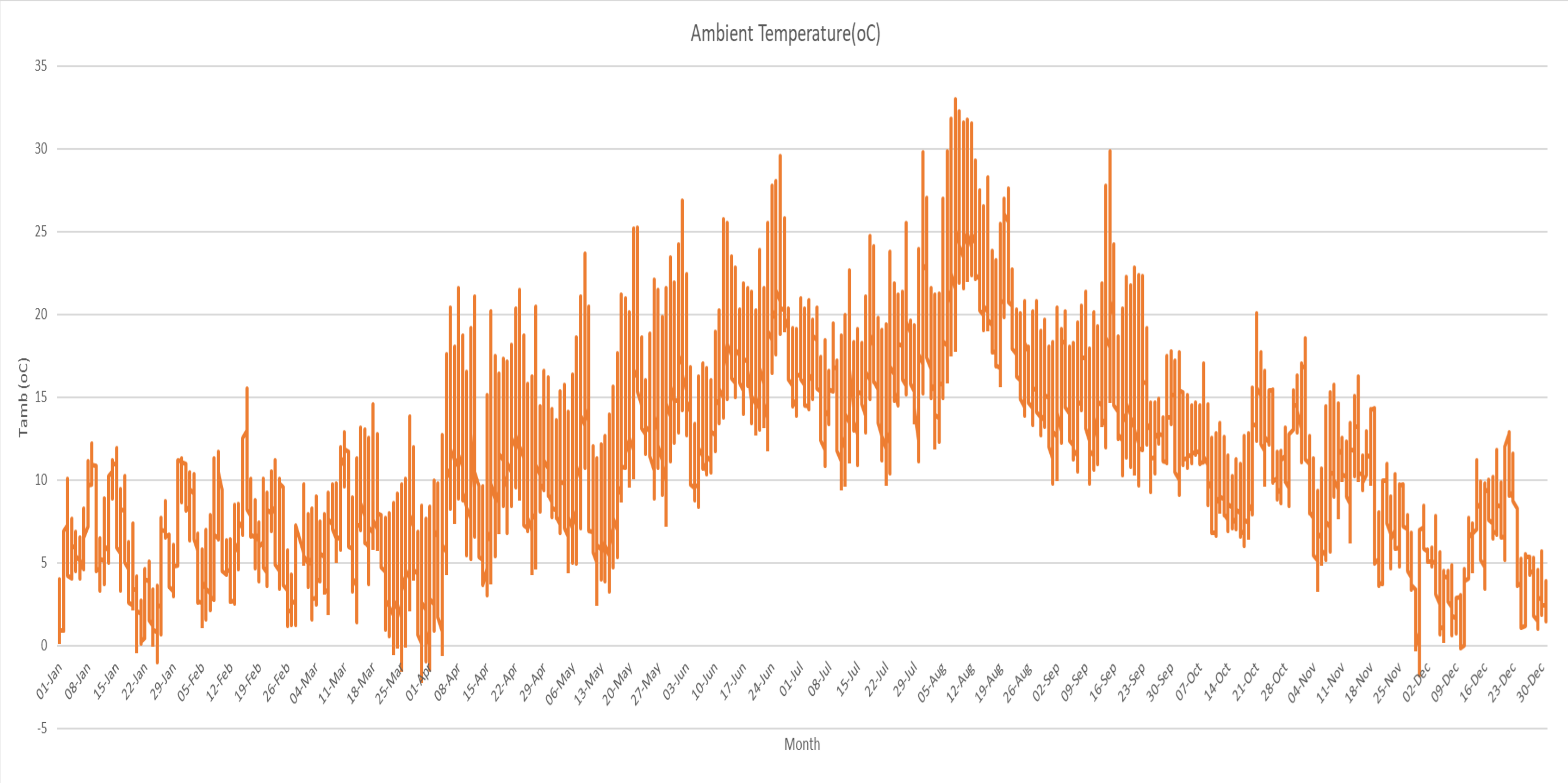

Figure 50: Ambient temperature data for whole year at Rosandepolder (*pvgis.com*, n.d.)

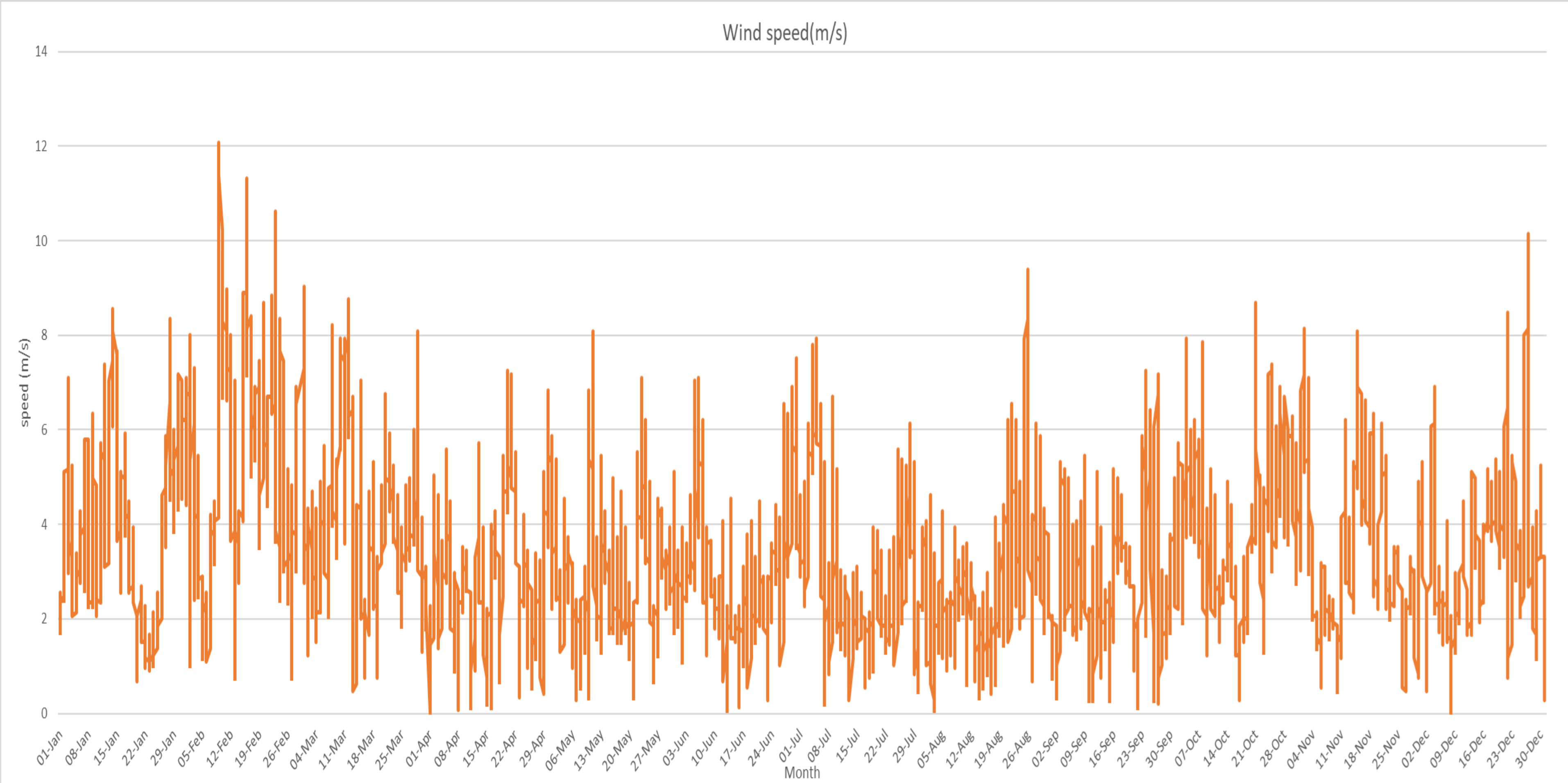

Figure 51: Wind speed at 10m at Rosandepolder (*pvgis.com*, n.d.)

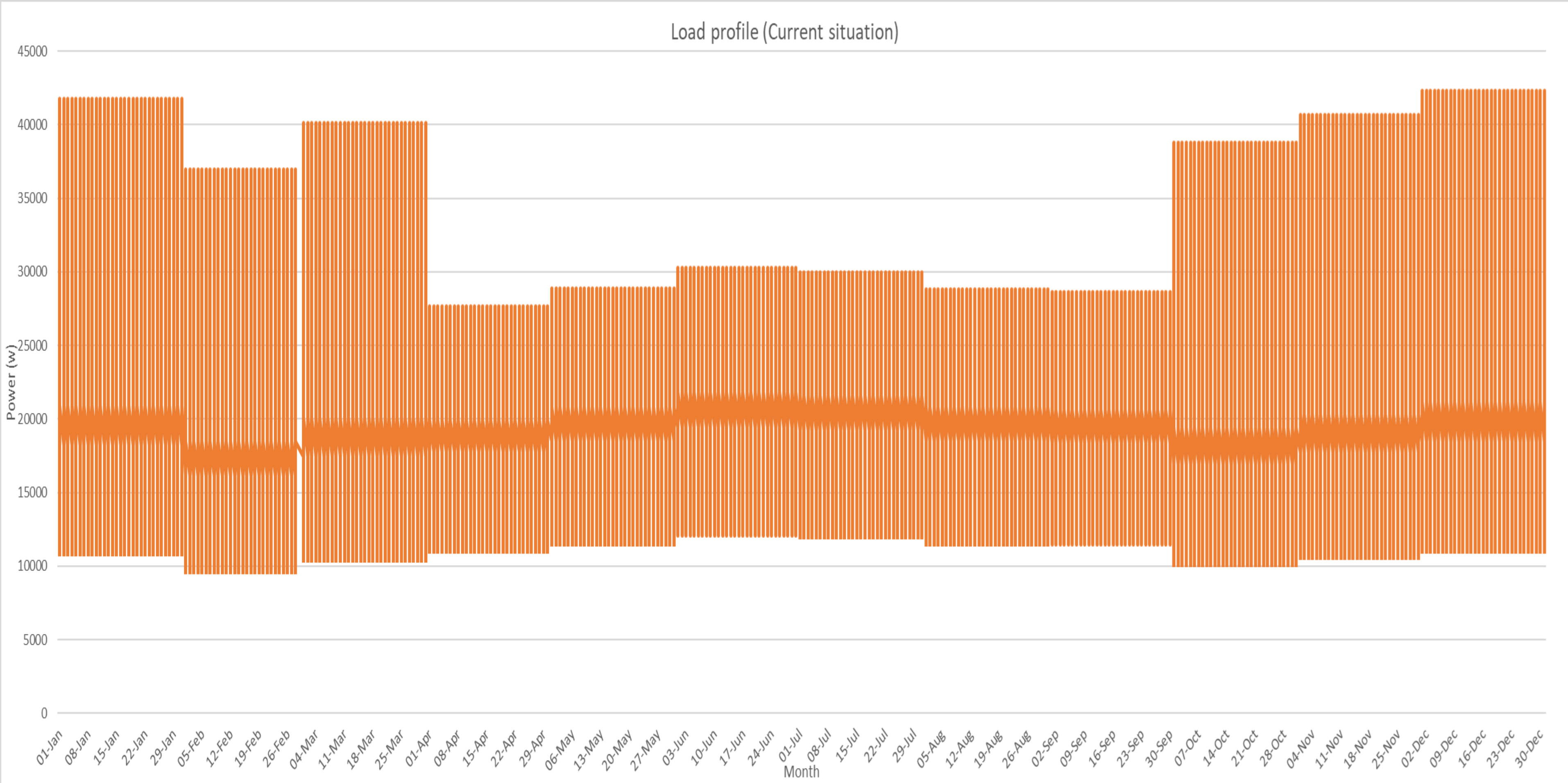

Figure 52: Load profile for scenario 1 and 2

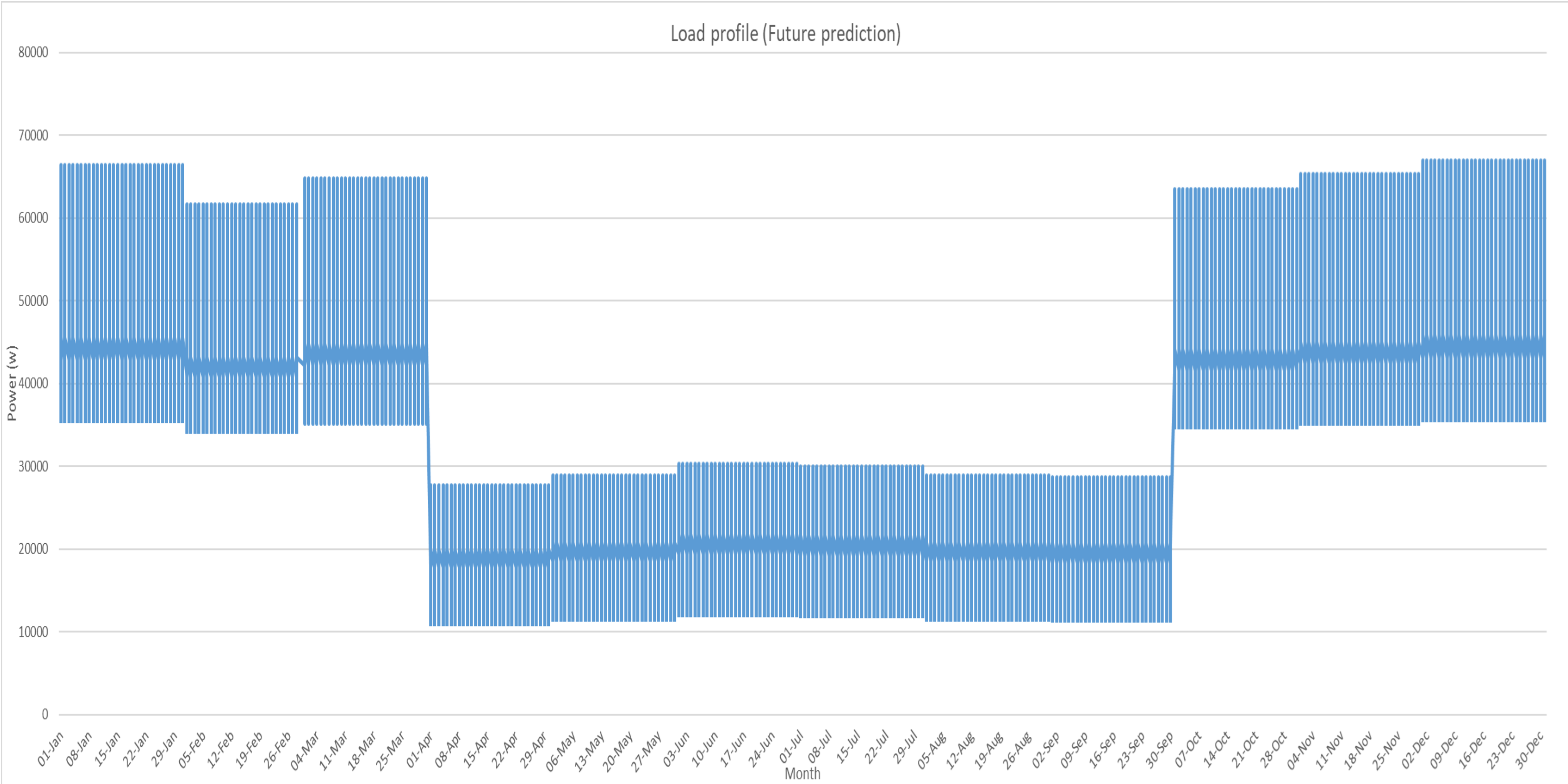

Figure 53: Load profile for scenario 3

APPENDIX E: Discounted Payback Period Calculation

Payback Period: **13.332 years**

Discounted Payback Period: **16.749 years**

Cash Flow Return Rate: **1.51% per year**

	Cash Flow	Net Cash Flow	Discounted Cash Flow	Net Discounted Cash Flow
Year 0	$-618,420.00	$-618,420.00	$-618,420.00	$-618,420.00
Year 1	$46,386.00	$-572,034.00	$45,166.50	$-573,253.50
Year 2	$46,386.00	$-525,648.00	$43,979.07	$-529,274.43
Year 3	$46,386.00	$-479,262.00	$42,822.85	$-486,451.57
Year 4	$46,386.00	$-432,876.00	$41,697.03	$-444,754.54
Year 5	$46,386.00	$-386,490.00	$40,600.81	$-404,153.73
Year 6	$46,386.00	$-340,104.00	$39,533.41	$-364,620.32
Year 7	$46,386.00	$-293,718.00	$38,494.07	$-326,126.25
Year 8	$46,386.00	$-247,332.00	$37,482.05	$-288,644.20
Year 9	$46,386.00	$-200,946.00	$36,496.64	$-252,147.56
Year 10	$46,386.00	$-154,560.00	$35,537.14	$-216,610.41
Year 11	$46,386.00	$-108,174.00	$34,602.86	$-182,007.55
Year 12	$46,386.00	$-61,788.00	$33,693.15	$-148,314.40
Year 13	$46,386.00	$-15,402.00	$32,807.35	$-115,507.05
Year 14	$46,386.00	$30,984.00	$31,944.84	$-83,562.21
Year 15	$46,386.00	$77,370.00	$31,105.00	$-52,457.21

Figure 54: Payback period calculation for scenario 1

Payback Period: **10.455 years**

Discounted Payback Period: **12.450 years**

Cash Flow Return Rate: **4.89% per year**

	Cash Flow	Net Cash Flow	Discounted Cash Flow	Net Discounted Cash Flow
Year 0	$-540,100.00	$-540,100.00	$-540,100.00	$-540,100.00
Year 1	$51,658.00	$-488,442.00	$50,299.90	$-489,800.10
Year 2	$51,658.00	$-436,784.00	$48,977.51	$-440,822.59
Year 3	$51,658.00	$-385,126.00	$47,689.88	$-393,132.70
Year 4	$51,658.00	$-333,468.00	$46,436.11	$-346,696.60
Year 5	$51,658.00	$-281,810.00	$45,215.30	$-301,481.30
Year 6	$51,658.00	$-230,152.00	$44,026.58	$-257,454.72
Year 7	$51,658.00	$-178,494.00	$42,869.11	$-214,585.61
Year 8	$51,658.00	$-126,836.00	$41,742.08	$-172,843.54
Year 9	$51,658.00	$-75,178.00	$40,644.67	$-132,198.87
Year 10	$51,658.00	$-23,520.00	$39,576.11	$-92,622.75
Year 11	$51,658.00	$28,138.00	$38,535.65	$-54,087.10
Year 12	$51,658.00	$79,796.00	$37,522.54	$-16,564.56
Year 13	$51,658.00	$131,454.00	$36,536.07	$19,971.51
Year 14	$51,658.00	$183,112.00	$35,575.53	$55,547.04
Year 15	$51,658.00	$234,770.00	$34,640.24	$90,187.28

Figure 55: Payback period calculation for scenario 2

Payback Period: **11.705 years**

Discounted Payback Period: **14.258 years**

Cash Flow Return Rate: **3.27% per year**

	Cash Flow	Net Cash Flow	Discounted Cash Flow	Net Discounted Cash Flow
Year 0	$-1,163,700.00	$-1,163,700.00	$-1,163,700.00	$-1,163,700.00
Year 1	$99,417.40	$-1,064,282.60	$96,803.70	$-1,066,896.30
Year 2	$99,417.40	$-964,865.20	$94,258.71	$-972,637.59
Year 3	$99,417.40	$-865,447.80	$91,780.64	$-880,856.95
Year 4	$99,417.40	$-766,030.40	$89,367.71	$-791,489.24
Year 5	$99,417.40	$-666,613.00	$87,018.22	$-704,471.02
Year 6	$99,417.40	$-567,195.60	$84,730.49	$-619,740.53
Year 7	$99,417.40	$-467,778.20	$82,502.92	$-537,237.61
Year 8	$99,417.40	$-368,360.80	$80,333.90	$-456,903.71
Year 9	$99,417.40	$-268,943.40	$78,221.91	$-378,681.80
Year 10	$99,417.40	$-169,526.00	$76,165.44	$-302,516.36
Year 11	$99,417.40	$-70,108.60	$74,163.04	$-228,353.32
Year 12	$99,417.40	$29,308.80	$72,213.28	$-156,140.04
Year 13	$99,417.40	$128,726.20	$70,314.78	$-85,825.26
Year 14	$99,417.40	$228,143.60	$68,466.19	$-17,359.06
Year 15	$99,417.40	$327,561.00	$66,666.21	$49,307.14

Figure 56: Payback period calculation for scenario 3